chemosensors

MDPI

Review

Silicon-Compatible Semiconductor Gas Sensors

Yanting Tang [1], Xinyi Chen [2,3,4], Huanhuan Zhang [2,3,4], Lanpeng Guo [2,3,4], Hua-Yao Li [2,3,4] and Huan Liu [2,3,4,*]

1 School of Integrated Circuit (School of Artificial Intelligence), Beijing Polytechnic University, Beijing 100176, China; yantingtang@bpu.edu.cn
2 School of Integrated Circuits, Huazhong University of Science and Technology, Wuhan 430074, China; acchenxinyi@hust.edu.cn (X.C.); huanhzhang@hust.edu.cn (H.Z.); guolanpeng@hust.edu.cn (L.G.); huayaoli@hust.edu.cn (H.-Y.L.)
3 Wuhan National Laboratory for Optoelectronics, Huazhong University of Science and Technology, Wuhan 430074, China
4 Optics Valley Laboratory, Wuhan 430074, China
* Correspondence: huan@hust.edu.cn

Abstract

The growing demand for intelligent environmental monitoring is driving the advancement of high-performance, low-cost, and highly integrated gas sensors. Silicon-compatible semiconductor gas sensors provide a promising platform to achieve this goal by leveraging their compatibility with complementary metal–oxide semiconductor (CMOS) processes. The established mass-manufacturing capabilities of micro-electromechanical systems (MEMS) and the high sensitivity and signal amplification characteristics of field effect transistors (FETs) in recent years have made the development of next-generation sensing devices feasible. In this review, we systematically summarize the latest advances in silicon-compatible gas sensors, with a focus on MEMS and FET technologies. We discuss their sensing mechanisms and performance optimization strategies, and further highlight the evolution of gas sensor technology toward on-chip intelligent olfactory systems that integrate sensing, computing, and storage capabilities.

Keywords: gas sensors; silicon-compatible; micro-electromechanical systems; field effect transistor; intelligent olfactory systems

Check for updates

Received: 30 December 2025
Revised: 30 January 2026
Accepted: 24 February 2026
Published: 17 March 2026

1. Introduction

Gas sensing technology plays an increasingly critical role in fields such as environmental monitoring, industrial safety, medical diagnosis, and smart homes [1–3]. With the deep integration of Internet of Things (IoT) and Artificial Intelligence (AI) technologies, the market has raised more urgent demands for high-performance gas sensors featuring low power consumption, miniaturization, and ease of system integration. Currently, metal oxide semiconductor gas sensors represented by companies such as Figaro, Sensirion, Bosch Sensortec, AMS, SGX Sensortech, and WinSen have become mainstream in applications like indoor air quality monitoring and flammable/explosive gas leak detection [4,5], owing to their mature fabrication processes and relatively stable performance. However, these sensors rely on traditional metal oxide sensing materials, which typically require operation at high temperatures to achieve effective response [6,7]. This results in high power consumption and severely limits their widespread adoption in emerging scenarios such as portable devices and large-scale sensor networks.

To overcome the power consumption bottleneck associated with high-temperature operation, silicon-compatible gas sensors are regarded as a highly promising development

 https://doi.org/10.3390/chemosensors14030070

direction [8–10]. This technological approach not only inherits the advantages of microelectromechanical systems processes in miniaturization and integration but also aims to achieve a balance between high performance and low power consumption through the synergistic innovation of sensing mechanisms and material systems. The technological evolution is chiefly driven along two core pathways: the miniaturization path via microelectromechanical systems (MEMS) and the mechanism innovation path utilizing field effect transistor (FET) architectures. Among these, MEMS-type gas sensors achieve a significant reduction in operating temperature and power consumption while maintaining performance through continuous optimization of micro-hotplate structures and sensitive materials [11,12]. FET-type gas sensors bring a fundamental breakthrough at the level of signal transduction mechanisms. They leverage gate voltage to effectively modulate the channel current, thereby amplifying the interaction between gas molecules and the sensitive material into significant electrical signal variations [13–15]. This enables the attainment of extremely high sensitivity and ultra-low detection limits.

Numerous studies have reviewed gas sensors from diverse perspectives [16–22]. For instance, Stamenkovic et al. comprehensively summarized the material systems and corresponding fabrication processes of semiconductor gas sensors [23]; Zhao focused on low-power metal oxide semiconductor gas sensors [24]; Li et al. focused on metal oxide CMOS-MEMS gas sensors based on the monolithic approach; Xia et al. systematically reviewed the progress in sensitive materials, modification methods, and manufacturing techniques for MEMS sensors targeting specific gases [25]; Ali et al. focused on gas sensors developed using MEMS technology and their applications [26]; Lee et al. systematically outlined the device structures and integration advantages of FET-type gas sensors [27]; Wan et al. examined the working principles and performance modulation of semiconductor nanowire field effect transistor gas sensors [28]; Filipovic et al. highlighted the application potential of two-dimensional materials in CMOS-integrated gas sensors [10]. Fan et al. systematically compared different types of sensors and their suitability for robotic applications [29]. These studies have collectively laid a crucial foundation for understanding the materials, devices, fabrication processes, and applications of gas sensors, each from the perspective of specific technological pathways or material systems.

Building on this foundation, this review aims to provide a more integrated and forward-looking perspective by systematically summarizes recent advances in silicon-compatible gas sensors. Particular focus is placed on examining the device architectures, sensing mechanisms, performance optimization, and integration strategies associated with MEMS and FET technologies. Furthermore, this paper explores the technological pathways in their intelligent evolution, particularly how artificial olfactory systems achieve high-throughput and high-precision analysis of complex gas environments through hardware array integration, virtual signal analysis, and sensing/storage/computing-integrated architectures. Finally, we provide an outlook on future trends in technological convergence and application expansion in this field.

2. MEMS-Type Gas Sensors

The technological evolution of semiconductor gas sensors is fundamentally reflected in the profound transformation of their form factor, size, and power consumption over the past four decades [18,30]. Early-generation sensors based on ceramic tube substrates, due to their high operating temperatures, typically suffered from large volume and high power consumption [31], making them unsuitable for high-density integration applications. To overcome these limitations, gas sensors have begun migrating to silicon-based platforms (Figure 1) [11,12,32–36]. Silicon-compatible technology delivers excellent mechanical stability and thermal conductivity, while also enabling seamless compatibility with standard integrated circuit processes. This lays a solid foundation for the miniaturization, low-power operation, and on-chip system integration of these sensors [37].

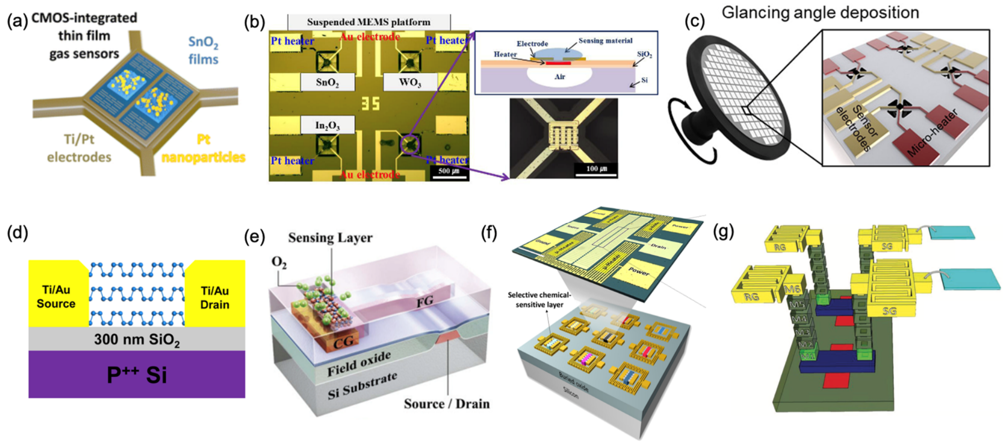

Figure 1. (**a**) MEMS device architecture fabricated via spray pyrolysis. Reprinted with permission from ref. [32]. (**b**) Low-power MEMS gas sensor array composed of SnO_2, WO_3, and In_2O_3 nanofibers prepared by EHD printing. Reprinted with permission from ref. [12]. (**c**) Schematic diagram of high-throughput uniform semiconductor metal oxide (SMO) gas sensors fabricated by glancing angle deposition (GLAD). Reprinted with permission from ref. [11]. (**d**) Schematic of a black phosphorus FET device. Reprinted with permission from ref. [33]. (**e**) Device structure of a Pt-In_2O_3 FET-type sensor. Reprinted with permission from ref. [34]. (**f**) Schematic of a chemically sensitive field effect transistor (CS-FET) chip. Reprinted with permission from ref. [35]. (**g**) Three-dimensional view of the proposed interdigital capacitive coupling structure. Reprinted with permission from ref. [36].

2.1. Structure and Gas-Sensing Mechanism

Serving as an interface between electronic systems and physical, chemical, and biological parameters [18], MEMS technology enables significant reductions in sensor volume, power consumption, and manufacturing costs, while enhancing on-chip integration with other functional components. Among the various technological approaches for silicon-compatible gas sensors, MEMS technology has emerged as a key pathway driving the evolution of gas sensors towards intelligent sensing chips, owing to its unique advantages in constructing three-dimensional microstructures and achieving thermal management and low power consumption [38,39]. Currently, gas sensors based on MEMS technology commonly employ metal oxide semiconductors (MOS) as the core sensing material [12,40], forming MEMS MOS gas sensors.

The core structure of MEMS MOS gas sensors lies in the silicon-based integration of high-performance gas-sensitive materials with micro-hotplates. The micro-hotplate, serving as the key supporting and heating unit, typically consists of a silicon substrate, a support layer, a micro-heater, and test electrodes. Owing to its small core area and low thermal mass, MEMS gas sensors exhibit significant advantages in terms of power consumption and thermal response speed. From the early closed-membrane structure, which effectively reduces heat loss [41], to the subsequently developed suspended-membrane structure that further optimizes heating efficiency and response time [42], the structural evolution of these sensors has directly driven their continuous performance enhancement.

Regarding the gas-sensing mechanism, MEMS MOS gas sensors rely on metal oxide semiconductor materials undergoing surface redox reactions with target gases under the high-temperature environment provided by the micro-hotplate. Taking a typical n-type semiconductor as an example [43], in air, oxygen molecules adsorb onto the material surface and capture conduction band electrons, forming an electron depletion layer that leads to increased resistance. When exposed to reducing gases, the gases react with the adsorbed oxygen, releasing electrons, which narrows the depletion layer and subsequently lowers the resistance. The response behavior of p-type semiconductors is the opposite.

This macroscopic electrical response is rooted in the complex interplay between microscopic defects in the material and gas–surface interactions. Specifically, the gas-sensing performance of metal oxide semiconductors is fundamentally linked to their intrinsic internal defects. Oxygen vacancies, serving as crucial donor defects, directly influence the baseline carrier concentration of the material. Under the high-temperature operating conditions maintained by the micro-hotplate, carriers are effectively excited, providing the foundation for high-sensitivity detection.

From a band theory perspective, the chemisorption of oxygen on the material surface forms a surface potential barrier, whose height and width modulate the transport behavior of bulk electrons [44]. For widely used polycrystalline nanomaterials, the Schottky barrier formed at grain boundaries acts as the primary controlling factor for resistance. When reducing gases react with surface-adsorbed oxygen, they release electrons into the material, thereby lowering the barrier height and narrowing the depletion layer, manifesting macroscopically as a decrease in resistance. This chain mechanism of constitutes the physical core of the gas-sensing behavior in metal oxide semiconductors.

2.2. Sensor Performance Optimization and Integration Strategies

The ongoing advancement of MEMS gas sensors is driven by two parallel forces: the stringent demands of high-volume commercial applications and the pursuit of advanced functionality for complex-scene analysis. In mass-market applications, the primary objective typically involves detecting specific target gases or simple gas mixtures using a single sensor. Representative scenarios include monitoring thermal runaway in lithium-ion batteries, detecting methane leaks, and controlling automotive ventilation systems. In these contexts, commercially available MEMS metal oxide semiconductor sensors (such as the Sensirion SGP series and Sciosense ENS160) demonstrate good performance, enabled by their highly optimized material formulations and integrated digital interfaces. In contrast, the research discussed in this section increasingly aims to overcome the inherent limitations of such commercial devices, targeting enhanced sensitivity/selectivity for trace gases, multi-gas analysis via sensor arrays, and on-chip integration of independently controlled sensing units—capabilities that remain largely at the laboratory or niche-product stage.

To achieve these distinct objectives, performance optimization proceeds along two interdependent fronts: material engineering and integration process innovation. In terms of materials, research has evolved from macro bulk materials towards micro/nanostructures. Since the discovery of the gas-sensitive properties of ZnO [45], researchers have successfully developed a variety of high-performance materials [46], including n-type SnO_2 [47], WO_3 [48,49], In_2O_3 [50,51], as well as p-type NiO [52] and CuO [53]. Notably, material morphology has progressed from early thick films and thin films to porous nanomaterials prepared by sol–gel, wet-chemical processes, and glancing angle deposition (GLAD) [54–56]. Their significantly increased specific surface area and abundant surface-active sites have substantially enhanced gas-sensing performance. For instance, CuO/WO_3 hierarchical hollow microspheres assembled from irregular nanosheets and synthesized via ultrasonic wet-chemical etching have been reported [49]. Their three-dimensional porous network provides abundant gas-accessible interfaces, resulting in a response to xylene approximately five times higher than that of pure WO_3. Recently, Jang et al. employed GLAD to fabricate Pd-modified WO_3 nanorods [56], which form vertically aligned porous array structures that effectively enhance hydrogen diffusion and surface contact, thereby achieving faster response and higher sensitivity. Such structurally optimized materials exhibit significantly enlarged specific surface areas and abundant active sites, leading to substantial improvements in gas-sensing performance.

The key to performance breakthroughs lies in the precise engineering of material surfaces and interfaces, with noble metal functionalization and heterojunction construction being two core strategies [40,57,58]. Noble metal modification primarily operates through electronic sensitization, where the catalytic dissociation of gas molecules on the noble metal surface triggers interface charge transfer. This alters the work function and modulates the height of the sensitive Schottky barrier formed at the metal–semiconductor junction, thereby amplifying the electrical signal. For example, Gao et al. developed a Pt-loaded SnO_2 nanoparticle sensor that achieved a 2.75-fold enhancement in response to toluene and a dramatic reduction in response time from 54 s to 5.4 s [59]. This improvement stems from the catalytic oxidation of toluene on the Pt nanoparticles and their role in modulating the surface electronic structure through charge transfer, both of which collectively enhance gas-sensing kinetics and signal magnitude. On the other hand, heterojunction engineering leverages the built-in electric field at the interface to enhance charge separation and transport [60], thereby significantly boosting sensing performance. Zhang et al. finely tuned the band structure of the NiO/ZnO p–n heterojunction by adjusting its composition ratio, enabling a sensor array to selectively distinguish multiple volatile organic compounds (VOCs) [61]. Furthermore, Zhou et al. demonstrated that their CeO_2/CuO n–p heterojunction significantly enhanced the H_2S response while also conferring excellent humidity tolerance and low-oxygen adaptability via interfacial synergy [62]. These studies demonstrate that precise interfacial design can simultaneously achieve high sensitivity, high selectivity, and high environmental robustness.

Simultaneous with material advancements is the continuous progress in MEMS micro-hotplate technology. Through the optimization of bulk micromachining and surface micromachining processes, the performance of micro-hotplates has been significantly enhanced. Specifically, optimizing the fabrication processes for heating electrodes and dielectric layers can effectively reduce device power consumption [63]; designing novel electrode geometries and heating methods improves temperature uniformity within the active area [64]; and the introduction of support structures like silicon islands significantly enhances the mechanical and thermal stability of the micro-hotplate while maintaining low power consumption [65].

However, the respective advantages of sensitive materials and micro-hotplates often struggle to achieve synergistic enhancement in high-performance sensing chips, with the core bottleneck being the integration challenge between the two. The traditional “fabricate micro-hotplate first, then transfer material” integration approach has distinct limitations. When using thin-film processes for localized deposition, the three-dimensional suspended structure of the micro-hotplate presents challenges for photolithographic patterning. Conversely, blanket deposition can lead to pad coverage and signal crosstalk issues, and the resulting films are often too dense, offering limited sensitivity. Alternatively, the transfer of nanomaterials synthesized via wet chemical methods faces problems such as insufficient material positioning accuracy, potential damage to the cantilever structure by the paste, and poor compatibility with standard MEMS processes.

To overcome this bottleneck, researchers have developed various integration strategies, the core of which lies in solving the challenges of material positioning and shaping on three-dimensional microstructures [66]. Based on the relationship between the material deposition/synthesis process and the micro-hotplate, these strategies can be broadly categorized into three representative technological pathways, which have seen significant progress in recent years.

The first is the direct deposition route based on micro-/nano-patterning techniques. The goal of this route is to achieve the patterned deposition of sensitive materials on the micro-hotplate surface. From the early sputtering techniques combined with physical masks [67] to later-developed direct-write/direct-print technologies like flame aerosol deposition [68], efforts have consistently focused on improving pattern resolution, film porosity, and process compatibility. Recently, researchers have further proposed a wafer-level integration strategy combining mask-assisted magnetron sputtering with atomic layer deposition [69]. As shown in Figure 2a, this method involves the precise patterned deposition of sensitive thin films, followed by the controlled modification with catalytic nanoparticles using atomic layer deposition technology. This ultimately results in the fabrication of a MEMS hydrogen sensing chip with a wide detection range (0.5~500 ppm), high resolution, and excellent consistency (Figure 2b), demonstrating the potential of this route for large-scale manufacturing.

The second route involves utilizing the micro-hotplate to induce in situ synthesis. This approach employs the micro-hotplate itself as a localized heat source to trigger chemical reactions through controlled heating, enabling the in situ and selective growth of sensitive materials in predetermined areas. Early work by the S. Semancik team demonstrated self-lithographic deposition of materials like SnO_2 and ZnO by driving chemical vapor deposition of precursors through localized heating on a micro-hotplate array [70]. Furthermore, integrating localized joule heating with microfluidic laminar flow technology [71] allows for the synthesis of heterogeneous nanomaterial arrays, which exhibit promising sensing performance towards gases such as NO_2 and CO. Recently developed localized self-heating aerosol-assisted chemical vapor deposition technology enables the direct growth of differentially functionalized nanomaterials on a monolithically integrated MEMS micro-array (Figure 2c) [72]. Gas-sensing tests reveal that this micro-array shows stable and reproducible responses to reducing gases like H_2, CO, and EtOH (Figure 2d), providing an efficient and low-cost solution for integrating multiple sensing units on a single chip.

The third is the route of precise integration of pre-fabricated materials based on micro/nanomanipulation. This approach aims to accurately integrate pre-synthesized, performance-optimized nanoscale sensitive materials into specific areas of the microhotplate using advanced micro/nanomanipulation techniques. Depending on the manipulation principles, it is primarily divided into two categories: guided assembly and direct transfer printing. In guided assembly, early studies utilized electric field manipulation or pre-deposited catalysts to guide the growth of nanowires at specific locations [26,73]. Meanwhile, using dielectrophoretic force to directionally assemble pre-synthesized nanoparticles into nanogap electrodes represents a more direct method for interface optimization, which can significantly enhance device sensitivity [74].

In direct transfer printing, micro/nanoprinting technology demonstrates strong process flexibility. For example, based on electrohydrodynamic (EHD) printing technology, metal oxide nanofiber inks can be precisely patterned onto suspended MEMS platforms to construct low-power sensor arrays [12]. Recently, this field has achieved breakthroughs in both materials and processes. Chen et al. through an innovative active colloidal polymer-directed method, successfully synthesized mesoporous SnO_2 nanospheres modified with single atoms [75], which were then used to formulate high-performance sensing inks. Using high-precision inkjet printing technology (Figure 2e), wafer-level, high-throughput (150 units/minute) patterned deposition can be achieved on MEMS micro-hotplates. The prepared sensors exhibited exceptional sensitivity (5.6 times higher than commercial sensors for 50 ppb ethanol) and excellent device-to-device consistency (coefficient of variation < 8.8%) (Figure 2f), demonstrating the great potential of the material manufacturing–performance co-optimization strategy.

https://doi.org/10.3390/chemosensors14030070

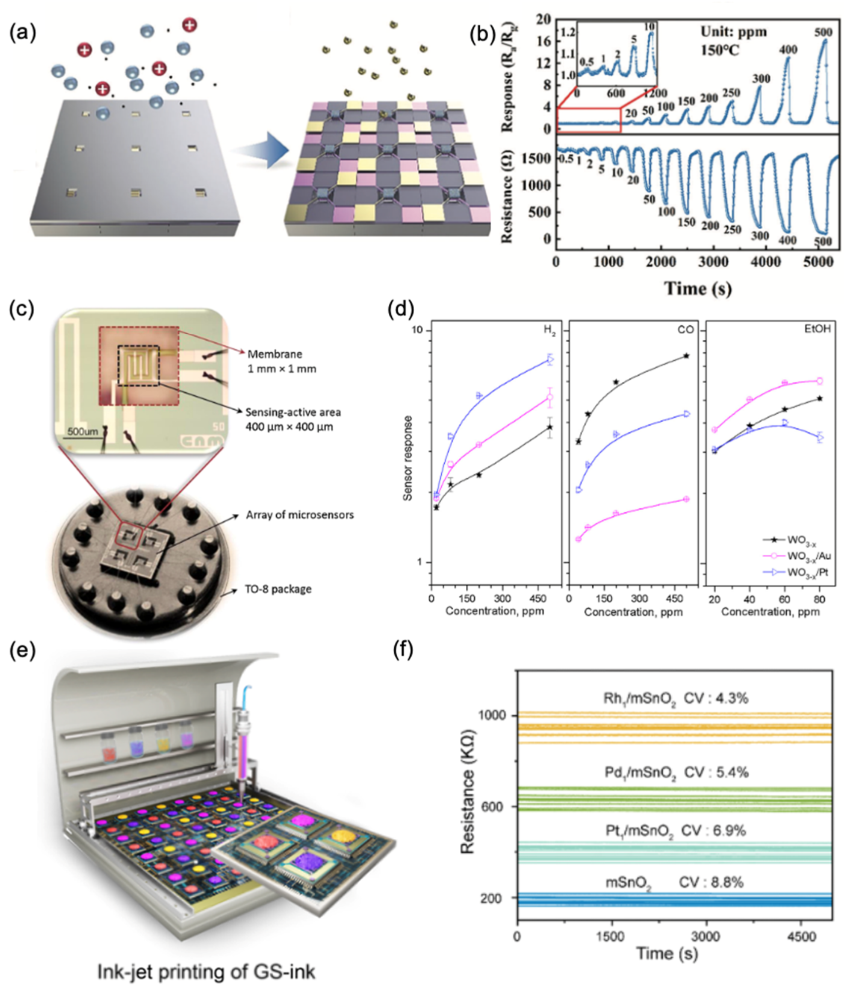

Figure 2. (**a**) Patterned deposition of a SnO_2 thin film in the central sensing region via mask-assisted magnetron sputtering. Reprinted with permission from ref. [69]. (**b**) Dynamic response of the sensing chip to hydrogen at concentrations ranging from 0.5 to 500 ppm, measured at 150 °C. Reprinted with permission from ref. [69]. (**c**) Optical micrograph of a single microsensor platform highlighting its sensitive active area. Reprinted with permission from ref. [72]. (**d**) Response characteristics of the sensor toward hydrogen (20, 80, 200, 500 ppm), carbon monoxide (40, 80, 200, 500 ppm), and ethanol (20, 40, 60, 80 ppm). Reprinted with permission from ref. [72]. (**e**) Optical image of the printed MEMS chip. Reprinted with permission from ref. [75]. (**f**) Excellent device-to-device resistance reproducibility demonstrated by the Pt/mSnO_2-based sensor. Reprinted with permission from ref. [75].

These sophisticated integration pathways represent significant strides in overcoming the material–process compatibility bottleneck. Nevertheless, it remains challenging to seamlessly merge the low power consumption and batch-manufacturing merits of MEMS devices with the high sensitivity and rapid response characteristics of sensitive materials for the reliable analysis of gases in complex, dynamic environments. Utilizing sensor arrays to address the issue of gas cross-sensitivity is an effective strategy. However, the integration density of current arrays is generally insufficient. The resulting large spatial separation can cause sensors at different positions to perceive varying gas concentrations, thereby compromising identification accuracy. Furthermore, most high-density arrays lack independent temperature control capability, which greatly limits their application potential. Therefore, developing on-chip, high-density sensing arrays with independent temperature control has become a crucial direction for enabling accurate and complex gas analysis.

3. FET-Type Gas Sensors

3.1. Structure and Gas-Sensing Mechanism

While MEMS MOS gas sensors have achieved widespread commercial success, FET gas sensors represent a distinct pathway where laboratory-scale breakthroughs have yet to translate broadly into mass-market products. To clearly delineate the technological distinctions between these two platforms, Table 1 summarizes their key characteristics across several performance and application metrics.

Table 1. Comparison of Typical MEMS-type gas sensors and FET-type gas sensors.

Aspect	MEMS-Type Gas Sensors	FET-Type Gas Sensors
Sensing Principle	Chemiresistive (surface resistance change)	Field effect modulation (threshold voltage, transconductance, etc.)
Typical Operating Temperature	Operation typically at 150–400 °C	Room temperature ~150 °C
Power Consumption	High (dominated by micro-heater, ~10–100 mW)	Very Low (μW to nW range, primarily electronic)
Detection Limit	ppm to ppb level	ppb to sub-ppb level (benefiting from intrinsic amplification)
CMOS Compatibility & Integration Level	High (mature MEMS processes, post-CMOS integration)	Very High (transistor-native, monolithic integration feasible)
Commercialization Status	Mature	Emerging/Lab-focused

The defining advantage of FET gas sensors lies in their unique signal transduction and amplification mechanism [27,76]. They utilize the gate voltage to modulate the channel current, achieving electrical signal amplification through the conductive channel formed at the gate dielectric/semiconductor interface. The interaction between gas molecules and the sensing layer significantly modulates multidimensional electrical parameters of the device, such as threshold voltage, transconductance, or mobility. These minute changes can be efficiently amplified by the FET's characteristic three-terminal structure, thereby enabling detection limits to reach the parts-per-billion (ppb) or even sub-ppb level [77]. This provides a new technological pathway for high-precision gas detection.

Based on the spatial position and functional role of the sensing layer within the device, FET gas sensors are primarily categorized into two fundamental configurations: channel-sensitive and gate-sensitive types [30,78]. In the channel-sensitive structure, the sensing material directly serves as the active layer of the conductive channel. Therefore, low-dimensional nanomaterials with excellent conductive properties are typically employed, such as carbon nanotubes [79–81], silicon nanowires [82,83], graphene [84–86], MoS_2 [87,88], black phosphorus [89], IGZO [90–93], and conductive organic polymers [94–96]. Research indicates that different low-dimensional materials possess distinct advantages in gas sensing.

In 2007, Novoselov's team pioneered the use of mechanically exfoliated graphene to fabricate a graphene field effect transistor (GFET) for NO_2 detection [97]. Graphene exhibits exceptionally high carrier mobility at room temperature, which facilitates efficient conduction of subtle charge variations. Combined with its ultra-low electrical noise characteristics, even single-molecule adsorption can induce a significant change in conductivity. With further investigation, the application of two-dimensional material systems in gas sensing has been significantly expanded. For instance, MoS_2 FETs, after optimization of layer numbers, have achieved highly sensitive detection of NO_2 at 20 ppb [98]. Black phosphorus FETs leverage their unique electronic structure to demonstrate ultra-low detection capabilities for NO_2 at 5 ppb at room temperature [33].

Gate-sensitive FETs adopt a more sophisticated structural design by physically separating the sensing layer from the conductive channel [99,100], effectively enhancing the device's long-term stability in complex environments. A typical example of such a structure can be traced back to the palladium gate FET hydrogen sensor proposed in 1975 [101]. With the advancement of micro/nanofabrication technology, this structure has undergone significant technical innovation. Mohammad Fahad et al. developed a CMOS-compatible Chemically Sensitive Field Effect Transistor (CS-FET) [35]. This design employs a 3.5 nm ultra-thin silicon channel and Ni-Pd as an ultra-thin chemically sensitive layer, achieving high sensitivity (~600%) for detecting 0.5% H_2 at room temperature. Building on this, Javey et al. further optimized the gate–channel coupling design [102]. By utilizing an ultra-thin sensing layer composed of Ni and Pd, they maximized capacitive coupling between the sensing layer and the channel, thereby generating a high response (>1000%) with low power consumption (<50 μW) to 0.5% H_2 gas at room temperature.

However, the traditional capacitive coupling mechanism is inherently limited by the physical isolation between the sensing layer and the channel. To overcome this bottleneck, the latest research proposes a revolutionary signal transduction mechanism based on an electron trapping effect. As shown in Figure 3a, this work constructed a silicon nanowire field effect transistor with a nano-air-gap gate (SiNW-NAG FET), where palladium nanoparticles (PdNPs) were deposited on the channel surface as the sensing layer [103]. When the thickness of the SiO_2 passivation layer was reduced to 2 nm, channel electrons could directly tunnel to and reach equilibrium with the PdNPs. The reaction of hydrogen with the PdNPs altered their energy level distribution (Figure 3b), breaking the equilibrium and triggering a dynamic electron trapping/release process between the channel and the nanoparticles, thereby achieving highly efficient signal transduction for hydrogen. This innovative mechanism enabled the sensor to exhibit record-high sensitivity (3600%/ppm), an ultra-low detection limit (4.4 ppb), and extremely low power consumption (~300 nW) at room temperature, while maintaining good selectivity and response speed (Figure 3c).

Compared to traditional metal-gate sensors, semiconductor gate-sensitive FET gas sensors combine the superior gas-sensing properties of semiconductor materials with the high transconductance advantage of field effect transistors, significantly expanding their detection capability for a variety of gases [104–107]. For example, a gate structure based on Pt/In_2O_3 enables precise monitoring of oxygen [34]. Constructing a ZnO FET with an interdigitated floating-gate structure [108] effectively increased the coupling area between the control gate and the floating gate, leading to a significant enhancement in NO_2 gas sensing performance at room temperature. Furthermore, the carbon nanotube floating-gate field effect transistor (FG FET) developed by Zhang et al. employed a Y_2O_3 dielectric layer and a Pd/WS_2 floating gate (Figure 3d) [109]. This device achieved a detection limit of 10 ppb for NO_2 at room temperature and exhibited excellent selectivity. When a visible-light-assisted mode was introduced, the sensor demonstrated complete recovery capability and stable humidity resistance within a 10~70% relative humidity range (Figure 3e,f). By flexibly replacing the floating-gate material, this architecture has been successfully applied to the detection of various gases including HCHO [110], toluene [81], H_2S [111], and NH_3 [112]. It shows promising platform scalability and environmental adaptability, laying a technical foundation for the development of multifunctional integrated sensing systems.

It is noteworthy that, apart from traditional high-κ dielectric materials like Y_2O_3, novel polymer electrolyte materials also offer new perspectives for the design of the dielectric layer in FET sensors. The side-gate FET (S-FET) gas sensor developed by Li et al. innovatively employs PVDF-HFP/[EMIM][TFSI] ionogel as the dielectric sensing layer (Figure 3g) [113], leveraging the electric double-layer capacitance changes induced by H_2S gas adsorption to modulate the channel current. Compared to conventional solid-state dielectric layers, this ionogel dielectric possesses unique bulk adsorption properties. Gas molecules can permeate its internal structure, leading to a significant capacitive response by altering ion mobility (Figure 3h). This sensor achieved highly sensitive detection of 20 ppb H_2S at room temperature. Furthermore, due to the hydrophobic nature of the ionogel, it maintained excellent stability across a 0~90% relative humidity range (Figure 3i). This work opens a new pathway for developing gas sensors with high interference resistance and low power consumption.

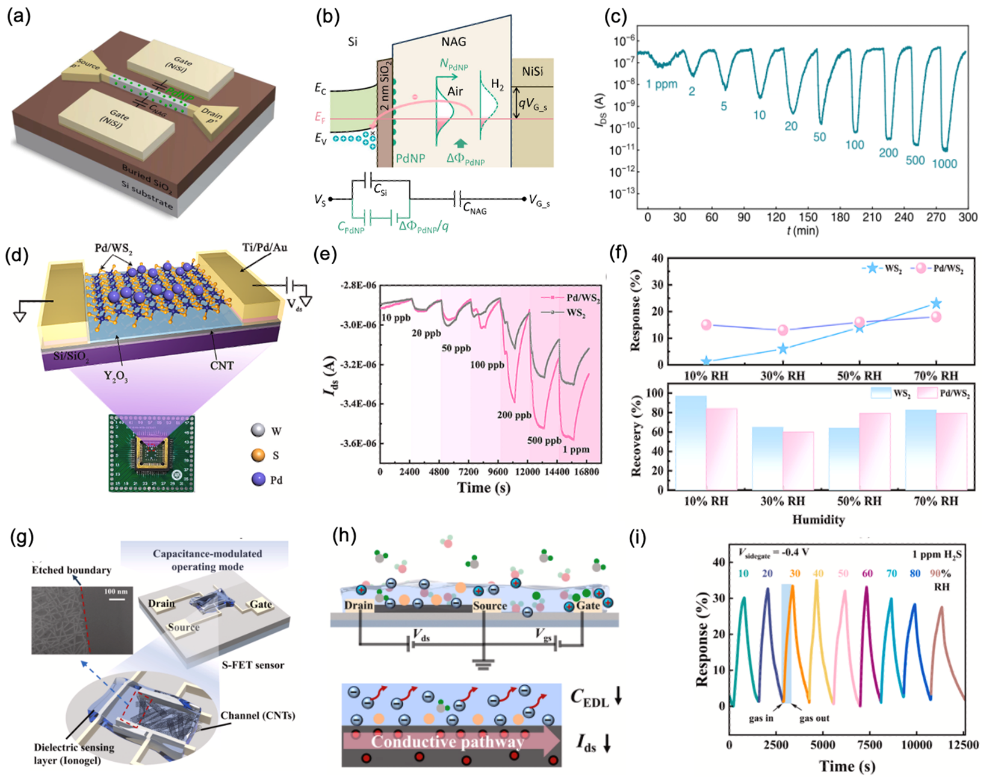

Figure 3. (**a**) 3D schematic of a silicon nanowire nanoscale air-gap FET (SiNW-NAG FET) for hydrogen detection. Reprinted with permission from ref. [103]. (**b**) Schematic of the SiNW-NAG FET with a 2 nm SiO_2 passivation layer under hydrogen exposure and its equivalent circuit. Reprinted with permission from ref. [103]. (**c**) Real-time detection of hydrogen at various concentrations at room temperature. Reprinted with permission from ref. [103]. (**d**) Schematic of a floating-gate FET (FG FET) sensor and a photograph of the packaged FG FET sensor chip. Reprinted with permission from ref. [109]. (**e**) Response and recovery curves of a WS_2-FET sensor and a Pd/WS_2-FET sensor exposed to NO_2 concentrations ranging from 10 to 1000 ppb. Reprinted with permission from ref. [109]. (**f**) Response and recovery ratios of WS_2-FET and Pd/WS_2-FET sensors under relative humidity (RH) conditions ranging from 10% to 70%. Reprinted with permission from ref. [109]. (**g**) Schematic and optical image of a side-gate FET (S-FET) sensor structure. Reprinted with permission from ref. [113]. (**h**) Schematic of the electric double-layer structure and the change in source–drain current after H_2S adsorption in a humid environment. Reprinted with permission from ref. [113]. (**i**) Effect of ambient humidity on H_2S sensing characteristics. Reprinted with permission from ref. [113].

This structural classification based on the spatial positioning of functional layers reflects the diversity in the design philosophy of FET gas sensors, providing clear technical pathways for device optimization tailored to different application scenarios. Ranging from the directly interacting channel-sensitive type to the physically isolated gate-sensitive type, sensors achieve a multi-dimensional balance among sensitivity, stability, and applicability, thereby driving the continuous advancement of gas sensing technology.

3.2. Performance Optimization and Multiparameter Strategies for Gas-Sensing Characteristics

Similar to MEMS gas sensors, the performance enhancement of FET-type gas sensors is fundamentally driven by innovations across two classic dimensions: material (surface/interface) engineering and device architecture. It is worth noting that the unique advantage of FET sensors lies in their inherent field effect tunability, which provides a more direct strategy for performance optimization.

The material engineering level, surface modification and heterojunction construction have become key strategies for enhancing the gas-sensing characteristics of FET gas sensors. Through rational material design and compositing, the sensitivity, selectivity, and stability of sensors can be effectively regulated. Noble metal modification is a classic method for improving the gas-sensing properties of materials [114]. Studies have shown that modifying the carbon nanotube channel surface with noble metal nanoparticles can significantly enhance its response sensitivity to NH_3 [112]. Similar surface engineering strategies have demonstrated significant effects in other material systems. For example, a graphene FET sensor modified with cobalt phthalocyanine (Figure 4a) [115] is used for high-sensitivity, high-selectivity detection of trace NO_2 in ambient air. This sensor utilizes cobalt phthalocyanine as a gas recognition receptor, which is uniformly modified onto the graphene surface via π-interactions. It achieves quantitative detection of NO_2 at the ppb level at room temperature, even under high humidity conditions, with a detection limit as low as 2 ppb (Figure 4b,c).

Heterojunction construction offers a richer design dimension for enhancing sensor performance. It has been reported that loading metal–organic framework materials onto MoS_2 to form a heterojunction leverages their porous properties to selectively enrich target gas molecules, thereby lowering the device's detection limit for NH_3 by an order of magnitude [116]. Expanding on this strategy, Salama et al. designed a heterojunction structure comprising PDVT-10 and a three-dimensional MOF (Figure 4d) [117], which served as the conductive channel of a thin-film transistor. In this design, the porous MOF acts as a specific pre-concentration layer for NO_2, and the heterojunction formed with the PDVT-10 semiconductor promotes interfacial charge transfer (Figure 4e), significantly enhancing the channel current response. As shown in Figure 4f, this sensor achieved a low detection limit of 8.25 ppb for NO_2 with a high sensitivity of 680 nA/ppb, representing a 700% performance improvement compared to a pure PDVT-10 device. It also exhibited excellent stability, reproducibility, and long-term reliability across a wide humidity range of 5~90%.

At the structural design level, innovations in gate engineering provide critical degrees of freedom for performance modulation. Novel device architectures are continuously emerging. For instance, a Z-gate tunnel field effect transistor employing a SiGe source region and a conductive polymer gate achieved a peak sensitivity of 5.65×10^5 towards chloroform, representing a four-fold improvement over traditional devices [118]. Furthermore, it is noteworthy that a structure has been reported utilizing a carbon nanotube channel with a Pd top-gate electrode for hydrogen sensing. This top gate, along with a Ta_2O_5/Y_2O_5 dielectric layer, forms a dual-gate configuration in conjunction with the underlying SiO_2/Si back gate (Figure 5a) [119]. By leveraging the capacitance asymmetry between the top-gate and back-gate dielectrics, the device achieves built-in signal amplification through capacitive coupling. This significantly enhanced the hydrogen sensitivity from 6.4 mV/ppm to 80 mV/ppm, far exceeding that of a conventional single-gate mode (Figure 5b,c). Similarly, Liu et al. integrated PbS quantum dots with the floating-gate structure of a GaAs HEMT, enabling highly sensitive detection of NO_2 through the capacitive coupling effect of the quantum dots [120].

Gate voltage modulation serves as a crucial optimization tool, significantly enhancing sensor performance by adjusting the channel potential. Zhou et al. constructed a gate-tunable sensing channel by combining MOF materials with 2D MoS_2. By modulating the back-gate voltage, they increased the NH_3 response by 22.48 times, achieving a response as high as 3303% to 100 ppm NH_3 at a −10 V gate bias [116]. Recently, Liu et al. further proposed a dual-gate modulation mechanism based on a PbS quantum dot/MoS_2 heterojunction (Figure 5d,e). This approach utilizes the capacitive coupling effect of quantum dots to introduce a gas-sensitive top-gate modulation to the MoS_2 channel, which works synergistically with the back-gate. At a back-gate voltage of 60 V, the device exhibited a response of 63.1 to 1 ppm NO_2 with a detection limit as low as 0.6 ppb, while the output current increased by three orders of magnitude (Figure 5f) [121]. External field modulation strategies provide additional dimensions for performance optimization. A ReS_2 FET sensor, through the synergistic regulation of light illumination and gate voltage, utilized wavelength selectivity to modulate carrier concentration, achieving highly selective detection of acetone (sensitivity of 4.34% ppm^{-1}) while maintaining stable performance for 30 days [105]. This optoelectronic co-modulation provides a new technological pathway for identifying specific gases in complex environments [122].

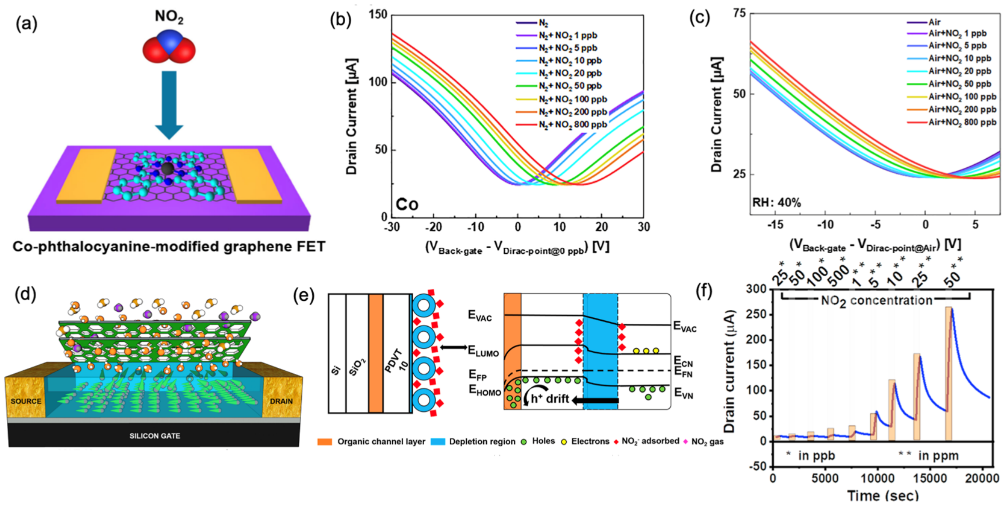

Figure 4. (**a**) Interaction mechanism between NO_2 gas and a graphene FET modified with Co-phthalocyanine. Reprinted with permission from ref. [115]. (**b**) Transfer characteristics of the Co-phthalocyanine modified graphene FET after introducing varying concentrations of NO_2 in a nitrogen atmosphere. Reprinted with permission from ref. [115]. (**c**) Transfer characteristics of the Co-phthalocyanine modified graphene FET upon exposure to NO_2 in air at 40% RH. Reprinted with permission from ref. [115]. (**d**) Schematic illustrating the interaction between NO_2 gas and the MOF-A/PDVT-10 organic field effect transistor (OFET) device. Reprinted with permission from ref. [117]. (**e**) Response mechanism of the MOF-A/PDVT-10 OFET device to NO_2. Reprinted with permission from ref. [117]. (**f**) Real-time response curve of the MOF-A/PDVT-10 OFET device under exposure to NO_2 concentrations ranging from 25 ppb to 50 ppm. Reprinted with permission from ref. [117].

With the advancement of artificial intelligence technology, FET gas sensors are rapidly evolving towards intelligence and multifunctionality. By integrating multidimensional sensing data with neural network algorithms, real-time analysis and concentration prediction of complex gas mixtures can be achieved. Furthermore, the emergence of flexible FET gas sensors expands their application prospects in wearable devices. Their integration with microfluidic technology has enabled the continuous monitoring of biomarker gases. These innovative directions fully demonstrate the immense application potential of FET gas sensors in fields such as environmental monitoring, medical diagnosis, and industrial safety.

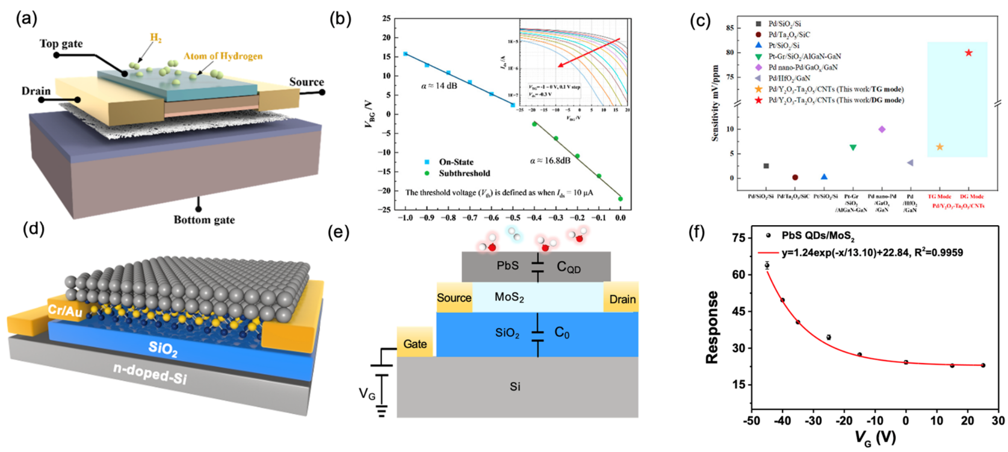

Figure 5. (**a**) Schematic structure of a dual-gate FET sensor. Reprinted with permission from ref. [119]. (**b**) Output characteristics measured via the back-gate as a function of top-gate voltage (V_{TG}). Reprinted with permission from ref. [119]. (**c**) Comparison of hydrogen sensor sensitivity based on the work function principle with previously reported data. Reprinted with permission from ref. [119]. (**d**) Schematic structure of a PbS quantum dots/MoS_2 thin-film transistor (TFT) gas sensor. Reprinted with permission from ref. [121]. (**e**) Circuit schematic of the PbS quantum dots/MoS_2 TFT gas sensor. Reprinted with permission from ref. [121]. (**f**) Gas-sensitive response of the 3.09 nm PbS quantum dots/MoS_2 TFT as a function of gate voltage (V_G). Reprinted with permission from ref. [121].

4. Artificial Olfactory Systems and Complex Scene Analysis

Accurate identification and quantification of specific components within complex gaseous environments is critical for applications in environmental monitoring, industrial safety, and medical diagnostics [123,124]. Most commercially available single-chip MOX sensors or small-scale arrays, which are typically designed for specific application scenarios, remain inadequate for the precise identification and quantification of components in complex gas mixtures. To overcome these limitations, artificial olfactory systems are dedicated to constructing a configurable sensing and analytical framework capable of addressing a broader range of highly complex gas mixtures. The field is currently undergoing a paradigm shift, evolving from discrete systems reliant on external processing units toward intelligent chip-based architectures that integrate sensing, storage, and computing functions.

Multi-dimensional signal acquisition and array construction form the foundation of a system's perceptual capability. On one hand, directly constructing arrays by integrating different sensing materials on a wafer is a straightforward method. For example, a wafer-scale gas sensor array based on carbon nanotube field effect transistors has been reported [125] (Figure 6a). By integrating four different sensing gate materials, it achieved simultaneous identification of various indoor hazardous gases such as NH_3, H_2S, and HCHO (Figure 6b–d). In a latest report, Ai et al. integrated nine carbon nanotube–metal oxide composite sensors onto an ultra-compact MEMS chip with an area of only 3 mm^2 [126], creating a high-density array. This was further integrated with readout circuits and advanced algorithms, and deployed on a smartphone platform, resulting in a portable pocket electronic nose capable of millisecond-level, low-power operation.

On the other hand, the inherent multidimensional electrical characteristics of FET devices provide an important foundation for constructing virtual arrays [127,128]. Sangaletti et al. developed an electronic nose system based on a graphene field effect transistor (GFET) [129]. By sweeping the gate voltage to obtain the complete transfer characteristic curve, the current responses at different bias points along the curve were treated as independent outputs of virtual sensors. Combined with data augmentation techniques and deep learning algorithms, this system achieved high-accuracy identification and discrimination of NH_3, NO_2, and their mixtures using only a single GFET. Compared with the traditional resistive readout mode, the sensitivity was enhanced by 20-fold, significantly simplifying the hardware architecture and system integration complexity. Furthermore, Liu et al. analyzed the electronic processes involved in gas–solid interface interactions and innovatively proposed an odor encoding method based on receptor function factors and transducer function factors (Figure 6e) [130]. This method was successfully applied to differentiate various oxidizing gases using quantum dot and black phosphorus thin-film transistors (Figure 6f,g). Furthermore, research on the low-frequency noise characteristics of CMOS-integrated FET gas sensors has found that their noise spectral features (e.g., corner frequency, amplitude) exhibit chemical specificity to gas types, serving as a unique noise fingerprint [131]. This implies that high-selectivity gas identification can be achieved without complex material modifications or multi-device arrays, but through in-depth analysis of the noise spectrum from a single device. This provides a novel hardware-minimalist paradigm for overcoming cross-sensitivity.

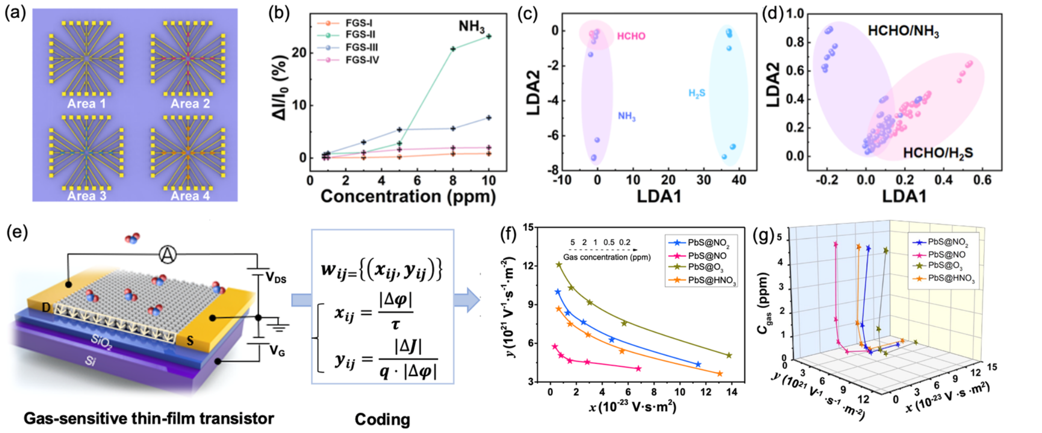

Figure 6. (**a**) Schematic diagram of the gas-sensitive sensor chip (GSC) comprising four distinct regions. Reprinted with permission from ref. [125]. (**b**) Response signals of the GSC to varying concentrations of the NH_3 gas. Reprinted with permission from ref. [125]. (**c**) Schematic of the Linear Discriminant Analysis (LDA) algorithm applied for discriminating three different target gases based on the sensor chip signals. Reprinted with permission from ref. [125]. (**d**) LDA distribution plot for classification of two categories of mixed gases using the sensor chip data. Reprinted with permission from ref. [125]. (**e**) Schematic illustrating the principle of odor-specific encoding with a single FET. Reprinted with permission from ref. [130]. (**f**) Two-dimensional response matrix of a PbS colloidal quantum dots TFT sensor to different oxidative gas concentrations, based on receptor function factor and transduction function factor analysis. Reprinted with permission from ref. [130]. (**g**) Three-dimensional odor space mapping of the PbS colloidal quantum dots TFT sensor under exposure to varying oxidative gas concentrations. Reprinted with permission from ref. [130].

With the advancement of device technology, emerging intelligent sensory units are gradually deepening the integration of sensing functions with memory and processing capabilities. Kong et al. proposed an amorphous chemiresistive gas sensor. Based on a $Ti/TiO_2/Pt$ structure [132], this device utilizes the selective modulation of oxygen vacancies by oxidizing and reducing gases for identification and possesses the ability to store the history of gas exposure, offering potential for sensing-computation integrated systems. Another study developed an olfactory-inspired in-sensor organic electrochemical transistor (OI-OECT) for a multimodal neuromorphic olfactory system (Figure 7a) [133]. Using p-type organic semiconductor material p(g2T-T) as the channel and combining it with an ion gel electrolyte, this device achieves tunable gas memory characteristics at low operating voltages, capable of mimicking typical neural behaviors such as inhibitory postsynaptic currents and paired-pulse facilitation. By modulating the gate voltage (0 V and −1 V), the device can transition from short-term memory to long-term memory and adjust the memory strength based on the duration, concentration, and interval of gas pulses (Figure 7b–d), simulating the cumulative damage effect of the human body to harmful gases.

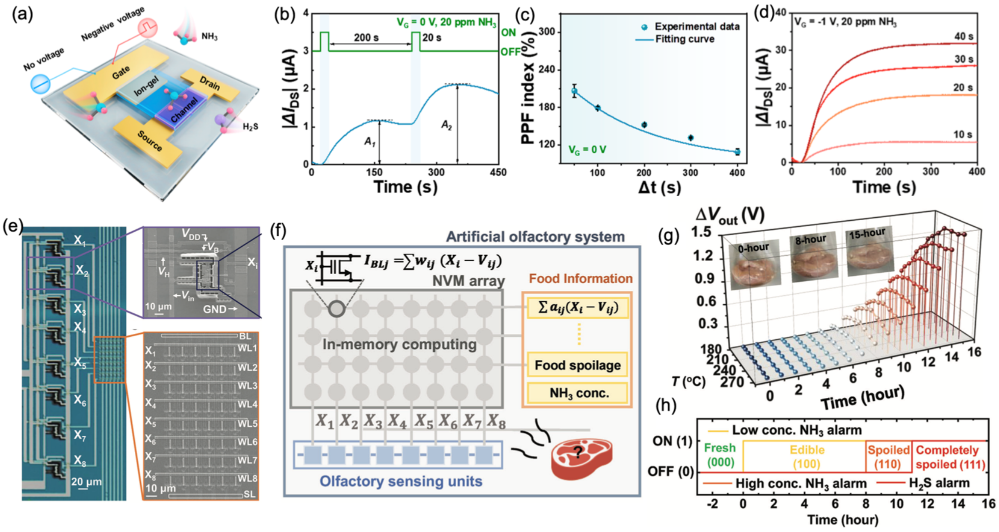

Figure 7. (**a**) Schematic diagram of the olfactory-inspired in-sensor organic electrochemical transistor (OI-OECT) with gate voltage tunability. Reprinted with permission from ref. [133]. (**b**) Typical paired-pulse facilitation (PPF) behavior induced by dual gas pulses (20 ppm NH_3, pulse width: 20 s, interval: 200 s). Reprinted with permission from ref. [133]. (**c**) PPF index as a function of pulse interval (20 ppm NH_3, 20 s) under a gate voltage of $V_G = 0$ V. Reprinted with permission from ref. [133]. (**d**) Gas memory characteristics regulated by pulse parameters (pulse interval: 20 s, 20 ppm NH_3) and gate voltage. Reprinted with permission from ref. [133]. (**e**) Optical micrograph of the artificial olfactory system (AOS). Reprinted with permission from ref. [134]. (**f**) Schematic illustration of the AOS architecture. Reprinted with permission from ref. [134]. (**g**) Transient response curves of ΔV_{out} during the spoilage process of chicken filet (inset shows photographs of the sample at different states). Reprinted with permission from ref. [134]. (**h**) Method for food status classification using the three-channel outputs of the AOS as binary signals. Reprinted with permission from ref. [134].

At the information processing level, the evolutionary path of technology is equally clear. In discrete architectures, from traditional methods like support vector machines (SVM) and principal component analysis (PCA) to advanced spatiotemporal deep learning models [135–138], powerful algorithms are key to analyzing array data and achieving accurate identification. However, to fundamentally reduce latency and power consumption, the research focus has shifted towards enabling computation through the hardware itself. Among these efforts, the near-sensor computing architecture integrates a FET gas sensor array and an AND-type non-volatile memory array on the same chip, achieving the integration of sensing and computing functions (Figure 7e) [134]. This system employs ZnO thin films as the gas-sensitive material, exhibiting high sensitivity (detection limit below 0.01 ppm) to food spoilage indicator gases NH_3 and H_2S. Eight sensing units operating at different temperatures form a differentiated gas response pattern. Leveraging in-memory computing technology, the system can directly perform linear combination processing on the sensor signals (Figure 7f), outputting a current signal linearly related to gas concentration. This enables real-time, continuous monitoring of food spoilage processes, such as in chicken (Figure 7g,h).

Furthermore, in the field of neuromorphic computing, research has employed devices like carbon nanotube (CNT) neuro-transistors to simulate the excitation inhibition regulation mechanism of biological olfaction at the hardware level [139]. Gas adsorption triggers excitatory synaptic currents, accomplishing cumulative memory of gas concentration; meanwhile, programmable ultraviolet light serves as an inhibitory signal to promote gas desorption, enabling autonomous system recovery and reset. This allows for suprathreshold alarm triggering without the intervention of an external processor.

In summary, through the synergistic development of multi-dimensional sensing hardware, intelligent device innovation, and integrated sensing–storage–computing architectures, artificial olfactory systems based on silicon-compatible gas sensors are continuously overcoming the bottleneck of cross-sensitivity. This lays a solid technical foundation for realizing their application in real-time, reliable, and low-power analysis within complex scenarios.

5. Conclusions

Driven by the parallel advancement of MEMS and FET technological pathways, silicon-compatible semiconductor gas sensors have emerged as a pivotal platform for high-performance gas detection, successfully integrating the key attributes of miniaturization, low power consumption, and high sensitivity. The MEMS approach, by monolithically integrating micromachined transducers (e.g., micro-hotplates) with silicon-based fabrication processes, has decisively addressed the historical challenges of high-power consumption and poor manufacturability in traditional sensors, enabling wafer-scale production with excellent uniformity. In parallel, FET-based sensors leverage their intrinsic electrical amplification and field effect tunability to offer unparalleled advantages in low-power, room-temperature operation, ultra-low detection limits, and the generation of multi-parameter response signatures for enhanced selectivity. Collectively, these technologies are transforming gas sensing from simple transducers into intelligent nodes capable of complex analysis.

Looking forward, the further development of silicon-compatible gas sensors will focus on heterogeneous functional integration and on-chip system intelligence. Realizing this vision will require overcoming several persistent technical bottlenecks. In terms of thermal management, thermoelectric crosstalk is a critical challenge in high-density integrated systems. In hybrid MEMS–FET structures or dense sensor arrays, heat generated by micro-hotplates can interfere with the electrical characteristics of adjacent sensitive circuits. Optimizing thermal isolation microstructures (e.g., suspended membranes, isolation trenches) and adopting time-multiplexed strategies to separate heating from sensing phases can effectively suppress thermal-coupling-induced signal distortion, offering a feasible pathway toward high-performance heterogeneously integrated systems.

At the same time, the long-term stability of sensors is crucial for their reliability and service life. Aging of sensitive materials and interference from complex environments can lead to gradual baseline drift, undermining the reliability of long-term monitoring. To address this, core–shell structures and surface passivation layers can be applied at the material level to improve intrinsic stability, while integrating reference sensors with adaptive correction algorithms at the system level enables real-time drift monitoring and compensation. Furthermore, on-chip self-calibration and batch-to-batch consistency are essential for scalable deployment. Conventional calibration methods relying on external standard gases are ill-suited to large-scale application needs. Future progress will depend on embedding miniaturized reference units on-chip, along with self-calibration algorithms based on environmental data and transfer learning, allowing sensors to perform autonomous calibration and parameter compensation in real-world environments. Advances in wafer-level testing and trimming technologies will also provide key manufacturing support for achieving inter-chip performance uniformity and enabling reliable mass-scale adoption.

https://doi.org/10.3390/chemosensors14030070

By achieving substantive breakthroughs in the above bottlenecks and promoting the co-development of novel sensing materials with silicon-compatible integration processes, gas-sensing technology will ultimately evolve toward fully integrated smart olfactory system-on-chip. Such chips will not only possess high-precision, multi-parameter sensing capabilities but will also integrate lightweight artificial intelligence algorithms to implement sensing–memory–computing integrated edge intelligence. These low-power, highly reliable intelligent sensing systems will provide core technical support for cutting-edge fields such as personalized health monitoring, real-time environmental sensing, industrial safety early warning, and the Internet of Things, empowering precise decision-making and dependable services in complex and dynamic environments.

Author Contributions: Conceptualization, H.L., Y.T., X.C., H.Z., L.G. and H.-Y.L.; investigation, Y.T.; writing—original draft preparation, Y.T.; writing—review and editing, H.L. and Y.T.; supervision, H.L. All authors have read and agreed to the published version of the manuscript.

Funding: This research was supported by the Fundamental Research Funds for Beijing Municipal Universities (No. 2025G011-KXQ), the Beijing Polytechnic University Research Project Funding, the 2025 General Project of Beijing Association of Higher Education (No. MS2025411), and the Maior Scientific and Technological Innovation Project of Wenzhou (No. ZG2023024).

Institutional Review Board Statement: Not applicable.

Informed Consent Statement: Not applicable.

Data Availability Statement: No new data were created or analyzed in this study.

Conflicts of Interest: The authors declare no conflicts of interest.

References

1. Zong, B.; Wu, S.; Yang, Y.; Li, Q.; Tao, T.; Mao, S. Smart Gas Sensors: Recent Developments and Future Prospective. *Nano-Micro Lett.* **2024**, *17*, 54. [CrossRef]
2. Chowdhury, M.A.Z.; Oehlschlaeger, M.A. Artificial Intelligence in Gas Sensing: A Review. *ACS Sens.* **2025**, *10*, 1538–1563. [CrossRef]
3. Nguyen, M.T.N.; Lee, J.S. Development of a Chemical Sensor Device for Monitoring Hazardous Gases Generated in the Semiconductor Manufacturing Process. *Chemosensors* **2024**, *12*, 233. [CrossRef]
4. Chai, H.; Zheng, Z.; Liu, K.; Xu, J.; Wu, K.; Luo, Y.; Liao, H.; Debliquy, M.; Zhang, C. Stability of Metal Oxide Semiconductor Gas Sensors: A Review. *IEEE Sens. J.* **2022**, *22*, 5470–5481. [CrossRef]
5. Gai, L.Y.; Lai, R.P.; Dong, X.H.; Wu, X.; Luan, Q.T.; Wang, J.; Lin, H.F.; Ding, W.H.; Wu, G.L.; Xie, W.F. Recent advances in ethanol gas sensors based on metal oxide semiconductor heterojunctions. *Rare Met.* **2022**, *41*, 1818–1842. [CrossRef]
6. Yu, S.; Jia, X.; Zhang, J.; Yang, W.; Song, H. Recent advances in different materials for moisture resistance of metal oxide-based gas sensors: A review. *Chem. Eng. J.* **2025**, *505*, 159639. [CrossRef]
7. Zhu, L.Y.; Ou, L.X.; Mao, L.W.; Wu, X.Y.; Liu, Y.P.; Lu, H.L. Advances in Noble Metal-Decorated Metal Oxide Nanomaterials for Chemiresistive Gas Sensors: Overview. *Nano-Micro Lett.* **2023**, *15*, 89. [CrossRef]
8. Sacco, L.; Forel, S.; Florea, I.; Cojocaru, C.-S. Ultra-sensitive NO_2 gas sensors based on single-wall carbon nanotube field effect transistors: Monitoring from ppm to ppb level. *Carbon* **2020**, *157*, 631–639. [CrossRef]
9. Mao, F.; Gui, J.; Zhu, Y.; Zeng, H.; Zhang, H. A CMOS-compatible and cost-effective room temperature sensitive hydrogen sensor. *Sens. Actuators B Chem.* **2024**, *418*, 136322. [CrossRef]
10. Filipovic, L.; Selberherr, S. Application of Two-Dimensional Materials towards CMOS-Integrated Gas Sensors. *Nanomaterials* **2022**, *12*, 3651. [CrossRef]
11. Kang, M.; Cho, I.; Park, J.; Jeong, J.; Lee, K.; Lee, B.; Del Orbe Henriquez, D.; Yoon, K.; Park, I. High Accuracy Real-Time Multi-Gas Identification by a Batch-Uniform Gas Sensor Array and Deep Learning Algorithm. *ACS Sens.* **2022**, *7*, 430–440. [CrossRef] [PubMed]
12. Kang, K.; Yang, D.; Park, J.; Kim, S.; Cho, I.; Yang, H.-H.; Cho, M.; Mousavi, S.; Choi, K.H.; Park, I. Micropatterning of metal oxide nanofibers by electrohydrodynamic (EHD) printing towards highly integrated and multiplexed gas sensor applications. *Sens. Actuators B Chem.* **2017**, *250*, 574–583. [CrossRef]

13. Shin, W.; Hong, S.; Jung, G.; Jeong, Y.; Park, J.; Kim, D.; Jang, D.; Park, B.-G.; Lee, J.-H. Improved signal-to-noise-ratio of FET-type gas sensors using body bias control and embedded micro-heater. *Sens. Actuators B Chem.* **2021**, *329*, 129166. [CrossRef]
14. Shin, W.; Jung, G.; Hong, S.; Jeong, Y.; Park, J.; Kim, D.; Park, B.-G.; Lee, J.-H. Optimization of channel structure and bias condition for signal-to-noise ratio improvement in Si-based FET-type gas sensor with horizontal floating-gate. *Sens. Actuators B Chem.* **2022**, *357*, 131398. [CrossRef]
15. Shin, W.; Jung, G.; Hong, S.; Jeong, Y.; Park, J.; Kim, D.; Jang, D.; Kwon, D.; Bae, J.H.; Park, B.G.; et al. Proposition of deposition and bias conditions for optimal signal-to-noise-ratio in resistor- and FET-type gas sensors. *Nanoscale* **2020**, *12*, 19768–19775. [CrossRef]
16. Kim, Y.J.; Woo, C.Y.; Kim, Y.; Kim, S.M.; Kim, N.Y.; Lee, H.W.; Oh, J.W. Recent progress of gas sensors toward olfactory display development. *Nano Converg.* **2025**, *12*, 42. [CrossRef]
17. Wei, J.; Peng, Q.; Xie, Y.; Chen, Y. Intelligent Gas Sensors: From Mechanism to Applications. *Sensors* **2025**, *25*, 6321. [CrossRef]
18. Liu, H.; Zhang, L.; Li, K.H.H.; Tan, O.K. Microhotplates for Metal Oxide Semiconductor Gas Sensor Applications-Towards the CMOS-MEMS Monolithic Approach. *Micromachines* **2018**, *9*, 557. [CrossRef]
19. Majhi, S.M.; Mirzaei, A.; Kim, H.W.; Kim, S.S.; Kim, T.W. Recent advances in energy-saving chemiresistive gas sensors: A review. *Nano Energy* **2021**, *79*, 105369. [CrossRef]
20. Nazemi, H.; Joseph, A.; Park, J.; Emadi, A. Advanced Micro- and Nano-Gas Sensor Technology: A Review. *Sensors* **2019**, *19*, 1285. [CrossRef]
21. Gardner, J.W.; Guha, P.K.; Udrea, F.; Covington, J.A. CMOS Interfacing for Integrated Gas Sensors: A Review. *IEEE Sens. J.* **2010**, *10*, 1833–1848. [CrossRef]
22. Akbari-Saatlu, M.; Procek, M.; Mattsson, C.; Thungstrom, G.; Nilsson, H.E.; Xiong, W.; Xu, B.; Li, Y.; Radamson, H.H. Silicon Nanowires for Gas Sensing: A Review. *Nanomaterials* **2020**, *10*, 2215. [CrossRef] [PubMed]
23. Nikolic, M.V.; Milovanovic, V.; Vasiljevic, Z.Z.; Stamenkovic, Z. Semiconductor Gas Sensors: Materials, Technology, Design, and Application. *Sensors* **2020**, *20*, 6694. [CrossRef] [PubMed]
24. Zhang, Y.; Li, R.; Guo, R.; Jiao, M.; Wang, G.; Zhao, Z. Recent Progress in Low-Power-Consumption Metal Oxide Semiconductor Gas Sensors. *Materials* **2025**, *18*, 4864. [CrossRef]
25. Wu, Y.; Lei, M.; Xia, X. Research Progress of MEMS Gas Sensors: A Comprehensive Review of Sensing Materials. *Sensors* **2024**, *24*, 8125. [CrossRef]
26. Santra, S.; Guha, P.K.; Ali, S.Z.; Hiralal, P.; Unalan, H.E.; Covington, J.A.; Amaratunga, G.A.J.; Milne, W.I.; Gardner, J.W.; Udrea, F. ZnO nanowires grown on SOI CMOS substrate for ethanol sensing. *Sens. Actuators B Chem.* **2010**, *146*, 559–565. [CrossRef]
27. Hong, S.; Wu, M.; Hong, Y.; Jeong, Y.; Jung, G.; Shin, W.; Park, J.; Kim, D.; Jang, D.; Lee, J.-H. FET-type gas sensors: A review. *Sens. Actuators B Chem.* **2021**, *330*, 129240. [CrossRef]
28. Feng, P.; Shao, F.; Shi, Y.; Wan, Q. Gas sensors based on semiconducting nanowire field-effect transistors. *Sensors* **2014**, *14*, 17406–17429. [CrossRef]
29. Zhang, W.; Tang, W.; Wan, Z.; Fan, Z. Advanced electronic noses for future robotic olfaction. *npj Robot.* **2026**, *4*, 11. [CrossRef]
30. Tang, Y.; Zhao, Y.; Liu, H. Room-Temperature Semiconductor Gas Sensors: Challenges and Opportunities. *ACS Sens.* **2022**, *7*, 3582–3597. [CrossRef]
31. Yamazoe, N. Toward innovations of gas sensor technology. *Sens. Actuators B Chem.* **2005**, *108*, 2–14. [CrossRef]
32. Sosada-Ludwikowska, F.; Reiner, L.; Egger, L.; Lackner, E.; Krainer, J.; Wimmer-Teubenbacher, R.; Singh, V.; Steinhauer, S.; Grammatikopoulos, P.; Koeck, A. Adjusting surface coverage of Pt nanocatalyst decoration for selectivity control in CMOS-integrated SnO_2 thin film gas sensors. *Nanoscale Adv.* **2024**, *6*, 1127–1134. [CrossRef] [PubMed]
33. Abbas, A.N.; Liu, B.; Chen, L.; Ma, Y.; Cong, S.; Aroonyadet, N.; Köpf, M.; Nilges, T.; Zhou, C. Black phosphorus gas sensors. *ACS Nano* **2015**, *9*, 5618–5624. [CrossRef] [PubMed]
34. Hong, S.; Shin, J.; Hong, Y.; Wu, M.; Jang, D.; Jeong, Y.; Jung, G.; Bae, J.H.; Jang, H.W.; Lee, J.H. Observation of physisorption in a high-performance FET-type oxygen gas sensor operating at room temperature. *Nanoscale* **2018**, *10*, 18019–18027. [CrossRef]
35. Fahad, H.M.; Shiraki, H.; Amani, M.; Zhang, C.; Hebbar, V.S.; Gao, W.; Ota, H.; Hettick, M.; Kiriya, D.; Chen, Y.-Z.; et al. Room temperature multiplexed gas sensing using chemical-sensitive 3.5-nm-thin silicon transistors. *Sci. Adv.* **2017**, *3*, e1602557. [CrossRef]
36. Tan, P.H.; Hsu, C.H.; Shen, Y.C.; Wang, C.P.; Liou, K.L.; Shih, J.R.; Lin, C.J.; Lee, L.; Wang, K.; Wu, H.M.; et al. Complementary Metal–Oxide–Semiconductor Compatible 2D Layered Film-Based Gas Sensors by Floating-Gate Coupling Effect. *Adv. Funct. Mater.* **2021**, *32*, 2108878. [CrossRef]
37. Hagleitner, C.; Hierlemann, A.; Lange, D.; Kummer, A.; Kerness, N.; Brand, O.; Baltes, H. Smart single-chip gas sensor microsystem. *Nature* **2001**, *414*, 293–296. [CrossRef]
38. Asri, M.I.A.; Hasan, M.N.; Fuaad, M.R.A.; Yunos, Y.M.; Ali, M.S.M. MEMS Gas Sensors: A Review. *IEEE Sens. J.* **2021**, *21*, 18381–18397. [CrossRef]
39. Huang, Y. Gas sensors on CMOS. *Nat. Electron.* **2025**, *8*, 197. [CrossRef]

40. Hsueh, T.J.; Ding, R.Y. A Room Temperature ZnO-NPs/MEMS Ammonia Gas Sensor. *Nanomaterials* **2022**, *12*, 3287. [CrossRef]
41. Suehle, J.S.; Cavicchi, R.E.; Gaitan, M.; Semancik, S.; Suehle, J.S. Tin Oxide Gas Sensor Fabricated Using CMOS Micro-Hotplates and in-Situ Processing. *IEEE Electron Device Lett.* **1993**, *14*, 118–120. [CrossRef]
42. Chan, P.; Yan, G.Z.; Sheng, L.Y.; Sharma, R.K.; Tang, Z.; Sin, J.K.O.; Hsinge, I.M.; Wang, Y. An Integrated Gas Sensor Technology Using Surface Micro-Machining. *Sens. Actuators B Chem.* **2002**, *82*, 277–283. [CrossRef]
43. Jeong, S.Y.; Kim, J.S.; Lee, J.H. Rational Design of Semiconductor-Based Chemiresistors and their Libraries for Next-Generation Artificial Olfaction. *Adv. Mater.* **2020**, *32*, e2002075. [CrossRef]
44. Degler, D.; Weimar, U.; Barsan, N. Current Understanding of the Fundamental Mechanisms of Doped and Loaded Semiconducting Metal-Oxide-Based Gas Sensing Materials. *ACS Sens.* **2019**, *4*, 2228–2249. [CrossRef]
45. Brattain, W.H.; Bardeen, J. Surface Properties of Germanium. *Bell Labs Tech. J.* **2013**, *32*, 1–41. [CrossRef]
46. Kim, H.-J.; Lee, J.-H. Highly sensitive and selective gas sensors using p-type oxide semiconductors: Overview. *Sens. Actuators B Chem.* **2014**, *192*, 607–627. [CrossRef]
47. Wang, C.; Li, R.; Feng, L.; Xu, J. The SnO_2/MXene Composite Ethanol Sensor Based on MEMS Platform. *Chemosensors* **2022**, *10*, 109. [CrossRef]
48. Wen, P.H.; Zheng, H.Y.; Hsueh, T.-J. A WO_3-NPs/MEMS NH_3 Gas Sensor. *J. Electrochem. Soc.* **2023**, *170*, 037506. [CrossRef]
49. Guo, M.; Luo, N.; Chen, Y.; Fan, Y.; Wang, X.; Xu, J. Fast-response MEMS xylene gas sensor based on CuO/WO_3 hierarchical structure. *J. Hazard. Mater.* **2022**, *429*, 127471. [CrossRef]
50. Kang, B.S.; Wang, H.-T.; Tien, L.-C.; Ren, F.G.; Brent, P.; Norton, D.P.; Abernathy, C.R.; Lin, J.; Pearton, S.J. Wide Bandgap Semiconductor Nanorod and Thin Film Gas Sensors. *Sensors* **2006**, *6*, 643–666. [CrossRef]
51. Hu, Y.; Liu, X.; Lin, W.; Yao, L.; Chen, L.; Zheng, C.; Feng, Y.; Gao, X. Development of MEMS gas sensors utilizing Ce-In_2O_3 nanostructures and optimized sensing films for enhanced acetone detection. *J. Alloys Compd.* **2025**, *1041*, 183885. [CrossRef]
52. Zhao, J.; Tan, Z.; Tian, B.; Zhao, L.; Zhao, F.; Wang, H. Low Concentration C_2H_2 Detection by NiO/SnO_2 Nanostructured Heterojunction Based MEMS Sensor. *J. Electrochem. Soc.* **2024**, *171*, 127503. [CrossRef]
53. Lai, L.-T.; Hsueh, H.-T.; Chiu, C.-H.; Cheng, T.-C.; Chang, S.-J. Thermal oxidation CuO nanowire gas sensor for ozone detection applications. *Sens. Actuators Rep.* **2024**, *8*, 100228. [CrossRef]
54. Zeng, Y.; Bing, Y.-F.; Liu, C.; Zheng, W.-T.; Zou, G.-T. Self-assembly of hierarchical $ZnSnO_3$-SnO_2 nanoflakes and their gas sensing properties. *Trans. Nonferr. Met. Soc. China* **2012**, *22*, 2451–2458. [CrossRef]
55. Liangyuan, C.; Shouli, B.; Guojun, Z.; Dianqing, L.; Aifan, C.; Liu, C.C. Synthesis of ZnO–SnO_2 nanocomposites by microemulsion and sensing properties for NO_2. *Sens. Actuators B Chem.* **2008**, *134*, 360–366. [CrossRef]
56. Park, S.J.; Lee, S.M.; Cho, S.H.; Kwon, H.R.; Kim, Y.; Yoo, D.J.; Hwang, I.S.; Jang, H.W. Chemoresistive and Catalytic Dual-Signal Pd-WO_3 MEMS Sensor for Reliable H_2 Monitoring. *Small* **2025**, *21*, e09377. [CrossRef]
57. Lin, Y.; Wang, Y.; Wei, W.; Zhu, L.; Wen, S.; Ruan, S. Synergistically improved formaldehyde gas sensing properties of SnO_2 microspheres by indium and palladium co-doping. *Ceram. Int.* **2015**, *41*, 7329–7336. [CrossRef]
58. Li, X.; Cho, J.H.; Kurup, P.; Gu, Z. Novel sensor array based on doped tin oxide nanowires for organic vapor detection. *Sens. Actuators B Chem.* **2012**, *162*, 251–258. [CrossRef]
59. Liu, X.; Zhao, J.; Wang, Y.; Hu, Y.; Xu, L.; Yao, L.; Zheng, C.; Yang, J.; Gao, X. Enhanced toluene gas-sensing properties of MEMS sensor based on Pt-loaded SnO_2 nanoparticles. *Nanotechnology* **2023**, *34*, 365502. [CrossRef]
60. Tong, J.; Lv, Y.; Zhuang, Z.; Yang, J.; Feng, B.; Zhao, J.; Huang, S.; Zhang, D.; Zhu, Y.; Cuniberti, G.; et al. Wafer-scale Pd-decorated Ta_2O_5/SnO_2 heterojunction sensor for ultrafast and sensitive hydrogen detection. *Sens. Actuators B Chem.* **2026**, *451*, 139432. [CrossRef]
61. Zhu, J.; Chen, L.; Ni, W.; Cheng, W.; Yang, Z.; Xu, S.; Wang, T.; Zhang, B.; Xuan, F. NiO/ZnO Nanocomposites for Multimodal Intelligent MEMS Gas Sensors. *ACS Sens.* **2025**, *10*, 2531–2541. [CrossRef]
62. Wang, Y.; Wang, M.; Jiang, X.; She, X.; Chen, Y.; Long, Y.; Zhou, Y. Deciphering the Humidity Resistance and Oxygen-Content Independence of Conductometric Hydrogen Sulfide Sensors Based on Electrospun CeO_2/CuO Nanotubes. *ACS Sens.* **2025**, *10*, 4262–4275. [CrossRef]
63. Solzbacher, F.; Imawan, C.; Steffes, H.; Obermeier, E.; Möller, H. A Modular System of SiC-Based Microhotplates for the Application in Metal Oxide Gas Sensors. *Sens. Actuators B Chem.* **2000**, *64*, 95–101. [CrossRef]
64. Wöllenstein, J.; Plaza, J.A.; Cané, C.; Min, Y.; Böttner, H.; Tuller, H.L. A novel single chip thin film metal oxide array. *Sens. Actuators B Chem.* **2003**, *93*, 350–355. [CrossRef]
65. Briand, D.; Krauss, A.; van der Schoot, B.; Weimar, U.; Barsan, N.; Göpel, W.; de Rooij, N.F. Design and Fabrication of High-Temperature Micro-Hotplates for Drop-Coated Gas Sensors. *Sens. Actuators B Chem.* **2000**, *68*, 223–233. [CrossRef]
66. Zhang, Z.; Zhang, Y.; Luo, Y.; Lv, G.; Yin, J.; Tan, P.; Duan, G. Wafer-Level Self-Assembly and Interface Passivation Patterning Technology for Nanomaterial-Compatible 3D MEMS Sensing Chips. *Nano-Micro Lett.* **2026**, *18*, 221. [CrossRef]
67. Wang, X.; Carey, W.P.; Yee, S.S. Monolithic Thin-Film Metal-Oxide Gas-Sensor Arrays with Application to Monitoring of Organic Vapors. *Sens. Actuators B Chem.* **1995**, *28*, 63–70. [CrossRef]

68. Tricoli, A.; Graf, M.; Mayer, F.; Kuehne, S.; Hierlemann, A.; Pratsinis, S.E. Micro-Patterning Layers by Flame Spray Aerosol Deposition. *Adv. Mater.* **2008**, *20*, 3005–3010. [CrossRef]
69. Zhang, Z.; Luo, L.; Zhang, Y.; Lv, G.; Luo, Y.; Duan, G. Wafer-Level Manufacturing of MEMS H_2 Sensing Chips Based on Pd Nanoparticles Modified SnO_2 Film Patterns. *Adv. Sci.* **2023**, *10*, e2302614. [CrossRef]
70. Semancik, S.; Cavicchi, R. Kinetically Controlled Chemical Sensing Using Micromachined Structures. *Acc. Chem. Res.* **1998**, *31*, 279–287. [CrossRef]
71. Yang, D.; Kang, K.; Kim, D.; Li, Z.; Park, I. Fabrication of heterogeneous nanomaterial array by programmable heating and chemical supply within microfluidic platform towards multiplexed gas sensing application. *Sci. Rep.* **2015**, *5*, 8149. [CrossRef] [PubMed]
72. Annanouch, F.E.; Gràcia, I.; Figueras, E.; Llobet, E.; Cané, C.; Vallejos, S. Localized aerosol-assisted CVD of nanomaterials for the fabrication of monolithic gas sensor microarrays. *Sens. Actuators B Chem.* **2015**, *216*, 374–383. [CrossRef]
73. Kumar, S.; Seo, Y.-K.; Kim, G.-H. Manipulation and Trapping of Semiconducting ZnO Nanoparticles into Nanogap Electrodes by Dielectrophoresis Technique. *Appl. Phys. Lett.* **2009**, *94*, 153104. [CrossRef]
74. Francioso, L.; De Pascali, C.; Creti, P.; Radogna, A.V.; Capone, S.; Taurino, A.; Epifani, M.; Baldacchini, C.; Bizzarri, A.R.; Siciliano, P.A. Nanogap Sensors Decorated with SnO_2 Nanoparticles Enable Low-Temperature Detection of Volatile Organic Compounds. *ACS Appl. Nano Mater.* **2020**, *3*, 3337–3346. [CrossRef]
75. Chen, K.; Zhu, L.; Wang, J.; Xie, W.; Deng, Y.; Xue, L.; Long, H.; Wan, H.; Ren, J.; Yuan, K.; et al. Active Polymer-Templated Porous Metal Oxide Nanospheres with Tailored Single-Atom Modification for Olfactory Intelligence. *J. Am. Chem. Soc.* **2025**, *147*, 47616–47626. [CrossRef] [PubMed]
76. Hong, Y.; Wu, M.; Bae, J.-H.; Hong, S.; Jeong, Y.; Jang, D.; Kim, J.S.; Hwang, C.S.; Park, B.-G.; Lee, J.-H. A new sensing mechanism of Si FET-based gas sensor using pre-bias. *Sens. Actuators B Chem.* **2020**, *302*, 127147. [CrossRef]
77. Shin, W.; Hong, S.; Jeong, Y.; Jung, G.; Park, J.; Kim, D.; Park, B.-G.; Lee, J.-H. Effects of Channel Length Scaling on the Signal-to-Noise Ratio in FET-Type Gas Sensor With Horizontal Floating-Gate. *IEEE Electron Device Lett.* **2022**, *43*, 442–445. [CrossRef]
78. Dong, M.-M.; He, H.; Zhao, M.-W.; Wang, C.-K.; Fu, X.-X. An ultra-sensitive and recyclable FET-type toxic gas sensor based on WTe2 monolayers. *J. Mater. Chem. A* **2024**, *12*, 26951–26961. [CrossRef]
79. Kong, J.; Franklin, N.; Zhou, C.; Chapline, M.; Peng, S.; Cho, K.; Dai, H. Nanotube molecular wires as chemical sensors. *Science* **2000**, *287*, 622–625. [CrossRef]
80. Hosseingholipourasl, A.; Syed Ariffin, S.H.; Rahimian Koloor, S.S.; Petru, M.; Hamzah, A. Analytical Prediction of Highly Sensitive CNT-FET-Based Sensor Performance for Detection of Gas Molecules. *IEEE Access* **2020**, *8*, 12655–12661. [CrossRef]
81. Zou, Q.; Liu, B.; Zhang, Y. Design of an array structure for carbon-based field-effect-transistor type gas sensors to accurately identify trace gas species. *J. Mater. Chem. A* **2023**, *11*, 15811–15820. [CrossRef]
82. Zafar, S.; D'Emic, C.; Jagtiani, A.; Kratschmer, E.; Miao, X.; Zhu, Y.; Mo, R.; Sosa, N.; Hamann, H.; Shahidi, G.; et al. Silicon Nanowire Field Effect Transistor Sensors with Minimal Sensor-to-Sensor Variations and Enhanced Sensing Characteristics. *ACS Nano* **2018**, *12*, 6577–6587. [CrossRef] [PubMed]
83. Verma, C.; Singh, J.; Tripathi, S.K.; Kumar, R. Design and Performance Analysis of Ultrathin Nanowire FET Ammonia Gas Sensor. *Silicon* **2021**, *14*, 6321–6327. [CrossRef]
84. Hayasaka, T.; Lin, A.; Copa, V.C.; Lopez, L.P., Jr.; Loberternos, R.A.; Ballesteros, L.I.M.; Kubota, Y.; Liu, Y.; Salvador, A.A.; Lin, L. An electronic nose using a single graphene FET and machine learning for water, methanol, and ethanol. *Microsyst. Nanoeng.* **2020**, *6*, 50. [CrossRef]
85. Hayasaka, T.; Kubota, Y.; Liu, Y.; Lin, L. The influences of temperature, humidity, and O_2 on electrical properties of graphene FETs. *Sens. Actuators B Chem.* **2019**, *285*, 116–122. [CrossRef]
86. Park, J.; Rautela, R.; Alzate-Carvajal, N.; Scarfe, S.; Scarfe, L.; Alarie, L.; Luican-Mayer, A.; Menard, J.M. UV Illumination as a Method to Improve the Performance of Gas Sensors Based on Graphene Field-Effect Transistors. *ACS Sens.* **2021**, *6*, 4417–4424. [CrossRef]
87. Zong, B.; Li, Q.; Chen, X.; Liu, C.; Li, L.; Ruan, J.; Mao, S. Highly Enhanced Gas Sensing Performance Using a 1T/2H Heterophase MoS_2 Field-Effect Transistor at Room Temperature. *ACS Appl. Mater. Interfaces* **2020**, *12*, 50610–50618. [CrossRef]
88. Yang, S.; Jiang, C.; Wei, S.-H. Gas sensing in 2D materials. *Appl. Phys. Rev.* **2017**, *4*, 021304. [CrossRef]
89. Aaryashree; Shinde, P.V.; Kumar, A.; Late, D.J.; Rout, C.S. Recent advances in 2D black phosphorus based materials for gas sensing applications. *J. Mater. Chem. C* **2021**, *9*, 3773–3794. [CrossRef]
90. Vijjapu, M.T.; Surya, S.G.; Yuvaraja, S.; Zhang, X.; Alshareef, H.N.; Salama, K.N. Fully Integrated Indium Gallium Zinc Oxide NO_2 Gas Detector. *ACS Sens.* **2020**, *5*, 984–993. [CrossRef]
91. Jayaswal, N.; Raman, A.; Kumar, N.; Singh, S. Design and analysis of electrostatic-charge plasma based dopingless IGZO vertical nanowire FET for ammonia gas sensing. *Superlattices Microstruct.* **2019**, *125*, 256–270. [CrossRef]

92. Shin, W.; Jeong, Y.; Hong, S.; Jung, G.; Park, J.; Kim, D.; Park, B.-G.; Lee, J.-H. Fully integrated FET-type gas sensor with optimized signal-to-noise ratio for H_2S gas detection. *Sens. Actuators B Chem.* **2022**, *367*, 132052. [CrossRef]
93. Jang, Y.-W.; Kang, J.; Jo, J.-W.; Kim, Y.-H.; Kim, J.; Park, S.K. Improved dynamic responses of room-temperature operable field-effect-transistor gas sensors enabled by programmable multi-spectral ultraviolet illumination. *Sens. Actuators B Chem.* **2021**, *342*, 130058. [CrossRef]
94. Hou, S.; Yu, J.; Zhuang, X.; Li, D.; Liu, Y.; Gao, Z.; Sun, T.; Wang, F.; Yu, X. Phase Separation of P3HT/PMMA Blend Film for Forming Semiconducting and Dielectric Layers in Organic Thin-Film Transistors for High-Sensitivity NO_2 Detection. *ACS Appl. Mater. Interfaces* **2019**, *11*, 44521–44527. [CrossRef]
95. Mougkogiannis, P.; Turner, M.; Persaud, K. Amine Detection Using Organic Field Effect Transistor Gas Sensors. *Sensors* **2020**, *21*, 13. [CrossRef]
96. Madan, J.; Pandey, R.; Chaujar, R. Conducting Polymer Based Gas Sensor Using PNIN- Gate All Around-Tunnel FET. *Silicon* **2020**, *12*, 2947–2955. [CrossRef]
97. Dong, M.M.; Fu, X.X.; Wang, C.K.; Zhao, M.W. Integration of High-Performance FETs and Sensitive Gas Sensors Using Janus $WSiGeP_4$ for Trace Toxic Gas Detection. *J. Phys. Chem. Lett.* **2025**, *16*, 3856–3867. [CrossRef]
98. Liu, B.; Chen, L.; Liu, G.; Abbas, A.N.; Fathi, M.; Zhou, C. High-performance chemical sensing using schottky-contacted chemical vapor deposition grown monolayer MoS_2 transistors. *ACS Nano* **2014**, *8*, 5304–5314. [CrossRef]
99. Jung, G.; Hong, Y.; Hong, S.; Jang, D.; Jeong, Y.; Shin, W.; Park, J.; Kim, D.; Jeong, C.B.; Kim, D.U.; et al. A low-power embedded poly-Si micro-heater for gas sensor platform based on a FET transducer and its application for NO_2 sensing. *Sens. Actuators B Chem.* **2021**, *334*, 129642. [CrossRef]
100. Shin, W.; Hong, S.; Jeong, Y.; Jung, G.; Park, J.; Kim, D.; Lee, C.; Park, B.G.; Lee, J.H. Effect of charge storage engineering on the NO_2 gas sensing properties of a WO_3 FET-type gas sensor with a horizontal floating-gate. *Nanoscale* **2021**, *13*, 9009–9017. [CrossRef]
101. Lundström, K.I.; Shivaraman, M.S.; Svensson, C.M. A hydrogen-sensitive Pd-gate MOS transistor. *J. Appl. Phys.* **1975**, *46*, 3876–3881. [CrossRef]
102. Fahad, H.M.; Gupta, N.; Han, R.; Desai, S.B.; Javey, A. Highly Sensitive Bulk Silicon Chemical Sensors with Sub-5 nm Thin Charge Inversion Layers. *ACS Nano* **2018**, *12*, 2948–2954. [CrossRef]
103. Hu, Q.; Solomon, P.; Osterlund, L.; Zhang, Z. Nanotransistor-based gas sensing with record-high sensitivity enabled by electron trapping effect in nanoparticles. *Nat. Commun.* **2024**, *15*, 5259. [CrossRef] [PubMed]
104. Jeong, Y.; Shin, J.; Hong, Y.; Wu, M.; Hong, S.; Kwon, K.C.; Choi, S.; Lee, T.; Jang, H.W.; Lee, J.-H. Gas sensing characteristics of the FET-type gas sensor having inkjet-printed WS_2 sensing layer. *Solid-State Electron.* **2019**, *153*, 27–32. [CrossRef]
105. Song, H.; Liu, J.; Lu, H.; Chen, C.; Ba, L. High sensitive gas sensor based on vertical graphene field effect transistor. *Nanotechnology* **2020**, *31*, 165503. [CrossRef] [PubMed]
106. Huang, Y.; Zhou, Y.; Liu, Y.; Chen, J.; Wei, X.; Cao, J. SnO_2/Carbon Nanotube Floating-Gate Field-Effect Transistor Gas Sensor for ppb-Level CO Detection. *ACS Appl. Nano Mater.* **2024**, *7*, 16119–16126. [CrossRef]
107. Jung, G.; Jeong, Y.; Hong, Y.; Wu, M.; Hong, S.; Shin, W.; Park, J.; Jang, D.; Lee, J.-H. SO_2 gas sensing characteristics of FET- and resistor-type gas sensors having WO_3 as sensing material. *Solid-State Electron.* **2020**, *165*, 107747. [CrossRef]
108. Hong, Y.; Kim, C.-H.; Shin, J.; Kim, K.Y.; Kim, J.S.; Hwang, C.S.; Lee, J.-H. Highly selective ZnO gas sensor based on MOSFET having a horizontal floating-gate. *Sens. Actuators B Chem.* **2016**, *232*, 653–659. [CrossRef]
109. Sun, Y.; Zhang, Y. Wafer-scale floating-gate field effect transistor sensor built on carbon nanotubes film for Ppb-level NO_2 detection. *Chem. Eng. J.* **2023**, *473*, 145480. [CrossRef]
110. Liu, C.; Hu, J.; Wu, G.; Cao, J.; Zhang, Z.; Zhang, Y. Carbon Nanotube-Based Field-Effect Transistor-Type Sensor with a Sensing Gate for Ppb-Level Formaldehyde Detection. *ACS Appl. Mater. Interfaces* **2021**, *13*, 56309–56319. [CrossRef]
111. Zhan, S.; Zuo, H.; Liu, B.; Xu, W.; Cao, J.; Zhang, Y.; Wei, X. Wafer-Scale Field-Effect Transistor-Type Sensor Using a Carbon Nanotube Film as a Channel for Ppb-Level Hydrogen Sulfide Detection. *ACS Sens.* **2023**, *8*, 3060–3067. [CrossRef] [PubMed]
112. Liu, J.; Hu, J.; Zhang, Y. A Carbon-Based FET-Type Sensor With Floating Sensing Gate for ppb-Level Ammonia Detection at Room Temperature. *IEEE Sens. J.* **2023**, *23*, 22180–22187. [CrossRef]
113. Li, Y.; Liu, B.; Zhang, Y. Novel working mode of FET gas sensor: Electric double layer capacitance modulation of ionogel dielectric sensing layer. *Chem. Eng. J.* **2025**, *516*, 164261. [CrossRef]
114. Park, S.-J.; Ha, T.-J. MoS_2 monolayers functionalized with gold nanoparticles using microwave absorption for FET-type NO_2 gas sensors in ppb-levels. *Appl. Surf. Sci.* **2023**, *622*, 156959. [CrossRef]
115. Kikawada, K.; Yazawa, N.; Nakanishi, R.; Maehashi, K.; Ikuta, T. Trace NO_2 Detection in Ambient Air Using Co-Phthalocyanine-Modified Graphene Field-Effect Transistors. *ACS Appl. Electron. Mater.* **2025**, *7*, 3828–3836. [CrossRef]
116. Wang, B.; Li, H.; Tan, H.; Gu, Y.; Chen, L.; Ji, L.; Sun, Z.; Sun, Q.; Ding, S.; Zhang, D.W.; et al. Gate-Modulated High-Response Field-Effect Transistor-Type Gas Sensor Based on the MoS_2/Metal-Organic Framework Heterostructure. *ACS Appl. Mater. Interfaces* **2022**, *14*, 42356–42364. [CrossRef]

https://doi.org/10.3390/chemosensors14030070

117. Yuvaraja, S.; Surya, S.G.; Chernikova, V.; Vijjapu, M.T.; Shekhah, O.; Bhatt, P.M.; Chandra, S.; Eddaoudi, M.; Salama, K.N. Realization of an Ultrasensitive and Highly Selective OFET NO_2 Sensor: The Synergistic Combination of PDVT-10 Polymer and Porphyrin-MOF. *ACS Appl. Mater. Interfaces* **2020**, *12*, 18748–18760. [CrossRef]
118. Dash, S. Design and sensitivity study of a novel Z-shaped gate TFET sensor with SiGe source for chemical analyte detection. *Phys. Scr.* **2024**, *99*, 0859a2. [CrossRef]
119. Qian, J.; Hua, Z.; Zhi, Z.; Sun, W.; Xiao, M.; Yang, S.; Xia, Y.; Sun, K.; Zhang, Z. Dual-Gate Field-Effect Transistor Ultrahighly Sensitive Hydrogen Sensors Enabled by an Ultrahigh Inherent Gain. *ACS Appl. Electron. Mater.* **2025**, *7*, 4938–4945. [CrossRef]
120. Hu, Z.; Zhou, L.; Li, L.; Ying, B.; Zhao, Y.; Wang, P.; Li, H.; Zhang, Y.; Liu, H. Quantum Dots-Sensitized High Electron Mobility Transistor (HEMT) for Sensitive NO_2 Detection. *Chemosensors* **2023**, *11*, 252. [CrossRef]
121. Tang, Y.; Zhou, B.; Liu, J.; Chen, X.; Wang, H.; Hu, Z.; Mao, R.; Xing, Y.; Li, H.Y.; Li, D.; et al. Dual-Gate Modulation in a Quantum Dots/MoS_2 Thin-Film Transistor Gas Sensor. *ACS Sens.* **2025**, *10*, 320–328. [CrossRef]
122. Zulkefli, A.; Mukherjee, B.; Sahara, R.; Hayakawa, R.; Iwasaki, T.; Wakayama, Y.; Nakaharai, S. Enhanced Selectivity in Volatile Organic Compound Gas Sensors Based on ReS_2-FETs under Light-Assisted and Gate-Bias Tunable Operation. *ACS Appl. Mater. Interfaces* **2021**, *13*, 43030–43038. [CrossRef] [PubMed]
123. Turlybekuly, A.; Shynybekov, Y.; Soltabayev, B.; Yergaliuly, G.; Mentbayeva, A. The Cross-Sensitivity of Chemiresistive Gas Sensors: Nature, Methods, and Peculiarities: A Systematic Review. *ACS Sens.* **2024**, *9*, 6358–6371. [CrossRef] [PubMed]
124. Mei, H.; Peng, J.; Wang, T.; Zhou, T.; Zhao, H.; Zhang, T.; Yang, Z. Overcoming the Limits of Cross-Sensitivity: Pattern Recognition Methods for Chemiresistive Gas Sensor Array. *Nano-Micro Lett.* **2024**, *16*, 269. [CrossRef] [PubMed]
125. Liu, C.; Xiao, Y.; Hu, J.; Hu, K.; Zhang, Y. Wafer-Scale Carbon-Based Field Effect Transistor Type Gas Sensor Array for Gaseous Mixture Identification. *ACS Sens.* **2025**, *10*, 5989–5998. [CrossRef]
126. Wang, X.; Kang, X.; Chen, X.; Xu, Y.; Ye, P.; Cui, J.; Ai, B. Pocket Electronic Nose Integrating an Ultra-Compact Sensor Array Chip and Spatiotemporal Network Enables Highly Selective Gas Sensing. *ACS Sens.* **2025**, *10*, 6887–6896. [CrossRef]
127. Torsi, L.; Dodabalapur, A.; Sabbatini, L.; PG, Z. Multi-parameter gas sensors based on organic thin-film-transistors. *Sens. Actuators B Chem.* **2000**, *67*, 312–316. [CrossRef]
128. Kumar, A.; Jha, P.; Singh, A.; Chauhan, A.K.; Gupta, S.K.; Aswal, D.K.; Muthe, K.P.; Gadkari, S.C. Modeling of gate bias controlled NO_2 response of the PCDTBT based organic field effect transistor. *Chem. Phys. Lett.* **2018**, *698*, 7–10. [CrossRef]
129. Zanotti, M.; Freddi, S.; Sangaletti, L. Physical Virtualization of a GFET for a Versatile, High-Throughput, and Highly Discriminating Detection of Target Gas Molecules at Room Temperature. *Adv. Mater. Technol.* **2024**, *10*, 2400985. [CrossRef]
130. Tang, Y.; Zhou, B.; Liu, J.; Guo, L.; Ying, B.; Chen, X.; Zhang, W.; Liang, Y.; Li, L.; Duan, Q.; et al. Specific Odor Coding Using a Single Thin-Film Transistor. *Nano Lett.* **2025**, *25*, 7587–7594. [CrossRef]
131. Lee, C.; Jeong, Y.; Koo, R.-H.; Cho, Y.; Choi, K.; Jung, G.; Kim, J.; Hong, S.; Im, J.; Lee, S.-T.; et al. Low-frequency noise in CMOS-integrated gas sensors: From a reliability constraint to a selective sensing feature. *Sens. Actuators B Chem.* **2026**, *446*, 138701. [CrossRef]
132. Kim, J.S.; Nam, Y.; Kim, D.Y.; Jang, N.; Kim, H.; Kim, S.D.; Vo, V.K.; Han, M.; Kong, S.H. Forming-free chemi-memristive gas sensing for artificial olfactory system. *Sens. Actuators B Chem.* **2025**, *444*, 138315. [CrossRef]
133. Yin, Y.; Sun, T.; Wang, L.; Li, L.; Guo, P.; Liu, X.; Xiong, L.; Zu, G.; Huang, J. In-Sensor Organic Electrochemical Transistor for the Multimode Neuromorphic Olfactory System. *ACS Sens.* **2024**, *9*, 4277–4285. [CrossRef] [PubMed]
134. Jung, G.; Kim, J.; Hong, S.; Shin, H.; Jeong, Y.; Shin, W.; Kwon, D.; Choi, W.Y.; Lee, J.H. Energy Efficient Artificial Olfactory System with Integrated Sensing and Computing Capabilities for Food Spoilage Detection. *Adv. Sci.* **2023**, *10*, e2302506. [CrossRef] [PubMed]
135. Zhang, H.; Zhang, Z.; Li, Z.; Han, H.; Song, W.; Yi, J. A chemiresistive-potentiometric multivariate sensor for discriminative gas detection. *Nat. Commun.* **2023**, *14*, 3495. [CrossRef]
136. Xiong, L.; He, M.; Hu, C.; Hou, Y.; Han, S.; Tang, X. Image presentation and effective classification of odor intensity levels using multi-channel electronic nose technology combined with GASF and CNN. *Sens. Actuators B Chem.* **2023**, *395*, 134492. [CrossRef]
137. Fang, C.; Li, H.-Y.; Li, L.; Su, H.-Y.; Tang, J.; Bai, X.; Liu, H. Smart Electronic Nose Enabled by an All-Feature Olfactory Algorithm. *Adv. Intell. Syst.* **2022**, *4*, 2270032. [CrossRef]
138. Khan, M.A.H.; Thomson, B.; Debnath, R.; Motayed, A.; Rao, M.V. Nanowire-Based Sensor Array for Detection of Cross-Sensitive Gases Using PCA and Machine Learning Algorithms. *IEEE Sens. J.* **2020**, *20*, 6020–6028. [CrossRef]
139. Jang, Y.W.; Kim, J.; Shin, J.; Jo, J.W.; Shin, J.W.; Kim, Y.H.; Cho, S.W.; Park, S.K. Autonomous Artificial Olfactory Sensor Systems with Homeostasis Recovery via a Seamless Neuromorphic Architecture. *Adv. Mater.* **2024**, *36*, e2400614. [CrossRef]